5-2011

Optimizing the performance of a glass-ceramic storage phosphor as an imaging plate for medical use

Manh Vu
mvu@utsi.edu

To the Graduate Council:

I am submitting herewith a thesis written by Manh Vu entitled "Optimizing the performance of a glass-ceramic storage phosphor as an imaging plate for medical use." I have examined the final electronic copy of this thesis for form and content and recommend that it be accepted in partial fulfillment of the requirements for the degree of Master of Science, with a major in Materials Science and Engineering.

Jacqueline A. Johnson, Major Professor

We have read this thesis and recommend its acceptance:

Charles E. Johnson, Zhongren Yue

Accepted for the Council:
Dixie L. Thompson

Vice Provost and Dean of the Graduate School

(Original signatures are on file with official student records.)

To the Graduate Council:

I am submitting herewith a thesis written by Manh Vu entitled “Optimizing the performance of a glass-ceramic storage phosphor as an imaging plate for medical use.” I have examined the final electronic copy of this thesis for form and content and recommend that it be accepted in partial fulfillment of the requirements for the degree of Master of Science, with a major in Materials Science and Engineering.

Jacqueline A. Johnson, Major Professor

We have read this thesis
and recommend its acceptance:

Charles E. Johnson

Zhongren Yue

Accepted for the Council:

Carolyn R. Hodges

Vice Provost and Dean of the Graduate School

(Original signatures are on file with official student records.)

Optimizing the performance of a glass-ceramic storage phosphor as an imaging plate for medical use

A Thesis Presented for the
Master of Science
Degree
The University of Tennessee, Knoxville

Manh Vu
May 2011

To my parents

ACKNOWLEDGEMENTS

This thesis is based upon studies of ZBLAN glasses from August 2009 to April 2011 at the Department of Materials Science and Engineering, The University of Tennessee Space Institute, Tullahoma, Tennessee.

I would like to thank my advisor Dr. Jacqueline A. Johnson for all of her guidance and support in successfully carrying out this work. I am very grateful for the help and patience of her husband, Dr. Charles E. Johnson over the last year. His experience in research and such considerable knowledge have been invaluable.

I would also like to thank Dr. Zhongren Yue for his support, intellectual and input for his participation in my Thesis Committee. I am also grateful to Dr. George M. Murray for the guidance, advice and useful discussions in my research.

I am grateful to Dr. Yuzi Liu and Dr. Amanda Petford-Long of Argonne National Laboratory for the TEM analysis. Alexander Terekhov, Kathleen Lansford, and Doug Warnberg have provided useful technical assistance.

I express my heartfelt thanks to my friends Amy Marquardt, Matthew Dede, Chris Foerster, Lee Leonard, Jason King and Deepak Rajput for their support during my time at UTSI €

ABSTRACT

Europium-doped-fluorochlorozirconate glass ceramics, known as ZBLAN, were produced in a glove box which has a controlled environment of argon gas. For imaging applications $BaCl_2$ is used instead of BaF_2. Their properties after different thermal processing and different amounts of europium-doping were investigated. After annealing the ZBLAN glass, $BaCl_2$ nanoparticles are precipitated in the glass matrix. These glass ceramic storage phosphors are strong candidates for replacing traditional x-ray screen film system and commercial storage phosphors such as Agfa MD-30.

Differential scanning calorimetry (DSC) was used to determine the crystallization temperature of the hexagonal phase of $BaCl_2$, and orthorhombic $BaCl_2$ this in turn determines the subsequent annealing temperature. X-ray diffraction (XRD) and photoluminescence (PL) show that the hexagonal phase of $BaCl_2$ was formed upon annealing at temperatures between 250 °C and 280 °C for 5 minutes. The orthorhombic phase of $BaCl_2$, which has storage properties, was formed at higher annealing temperatures, at approximately 290 °C and above. Secondary ion mass spectroscopy (SIMS) was used to determine adsorbed/diffused oxygen content of the glass. The weight loss of fluorine and chlorine is 3-5 % and was determined using ion chromatography (IC). The concentration of other cations was determined using inductively coupled plasma spectroscopy (ICP). Transmission electron microscopy (TEM) was used to take high resolution pictures and verify the composition of $BaCl_2$ nanoparticles. The relative concentration of Eu^{2+} to Eu^{3+} of heated $EuCl_3$ and ZBLAN was studied using Mössbauer spectroscopy. The oxidation of Eu^{2+} to Eu^{3+} was also observed during the experiment. This study has reinforced the strong potential for application of glass-ceramic storage phosphors for medical imaging.

TABLE OF CONTENTS

Chapter Page

LIST OF TABLES

Table Page

LIST OF FIGURES

Figure Page

CHAPTER I
INTRODUCTION AND BACKGROUND

1.1 Introduction

The medical and photovoltaic industries have great interest in fluorozirconate-based glass ceramics. Fluorozirconate-based glass ceramics, which are doped with rare-earths, could be used for medical imaging because of its storage properties, down-converting top layers or up-converting back layers of solar cells for enhancing their efficiency. Storage phosphor materials are the most successful digital detectors for replacing traditional film-screen systems in medical imaging applications [1]. The advantages of glass-ceramic storage phosphors are mostly due to their large dynamic range, easy portability, and lower cost [2]. Increased sensitivity of the glass-ceramic storage phosphor can reduce the x-ray dose to lower levels while maintaining the high image quality. The spatial resolution of the glass-ceramic storage phosphor is much higher compared to other methods due to the size of precipitated $BaCl_2$ nanoparticles. Various studies have been developed to minimize light scattering during the readout process to improve the spatial resolution of glass-ceramic storage phosphor image plates.

1.2 Commercial Storage Phosphor vs. Traditional Film-screen System

Figure 1 below describes the principle difference between the traditional film-screen system and the storage phosphor for medical imaging. X-rays were first discovered in 1895 and were used immediately in conventional x-ray imaging. When a photographic film is x-irradiated, a special phosphor coating on the film glows and exposes the film. The x-ray image becomes visible after appropriate chemical processing of the film much like a regular photograph. The energy and wavelength of the x-rays allow them to pass through the soft tissue part of the body more easily, while passing

through bones, clogged blood vessels, or dense matter is more difficult. The differences in brightness and contrast create an image of internal body structures.

Storage phosphors are commercially the most successful digital detectors for replacing film-screen systems before the innovation of its competitor, a glass-ceramic storage phosphor. X-ray storage phosphors contain crystallites embedded in an organic binder. When the storage phosphor is x-irradiated, it can convert ionizing radiation into stable electron-hole pairs in these crystallites [3]. The defects generated should be stable at room temperature to make sure the image information is stored until it is read out (approximately 4-6 hours). The digital images can be read out by scanning a laser beam to activate recombination of the electron-hole pairs, which leads to photostimulated luminescent emission (PSL). Furthermore, storage phosphor image plates are compatible with X-ray equipment already in place. Reading devices are durable and can be centrally located to help increase access and reduce costs.

In Figure 2a, an electron is stimulated from the valence band (VB) to the conduction band (CB) due to incoming x-rays. Its relaxed energy level traps and creates an electron-hole pair. In Figure 2b, the incoming laser beam helps an electron get out of the energy level trap to recombine with the hole.

Figure 3 describes the cycle for using a storage phosphor plate. After the image is stored on a storage phosphor plate, it is sent to a reading device. The signal is enhanced using a photo multiplier tube and the digital image is saved in the computer. The storage phosphor plate can then be erased under a halogen lamp. The whole process takes a few minutes and the storage phosphor plate is ready to be used for the next patient.

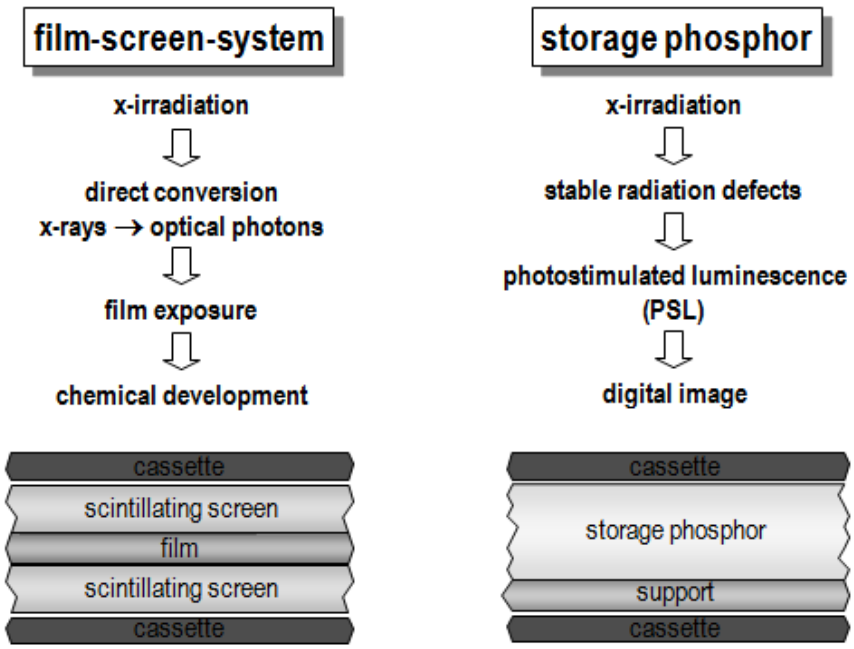

Figure 1 Principle of film-screen system vs. BaFBr doped with Eu^{2+} [4]

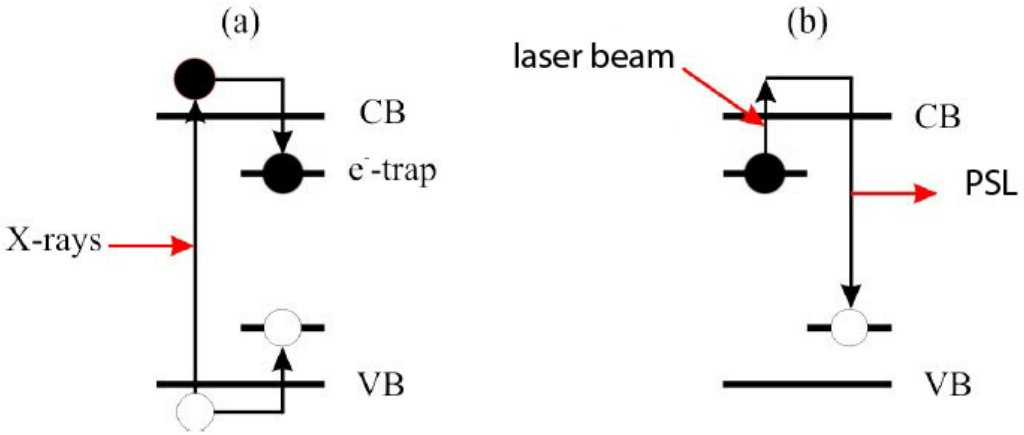

Figure 2 a) Schematic of electron hole pair generation, b) Schematic of photostimulated luminescent emission (PSL).

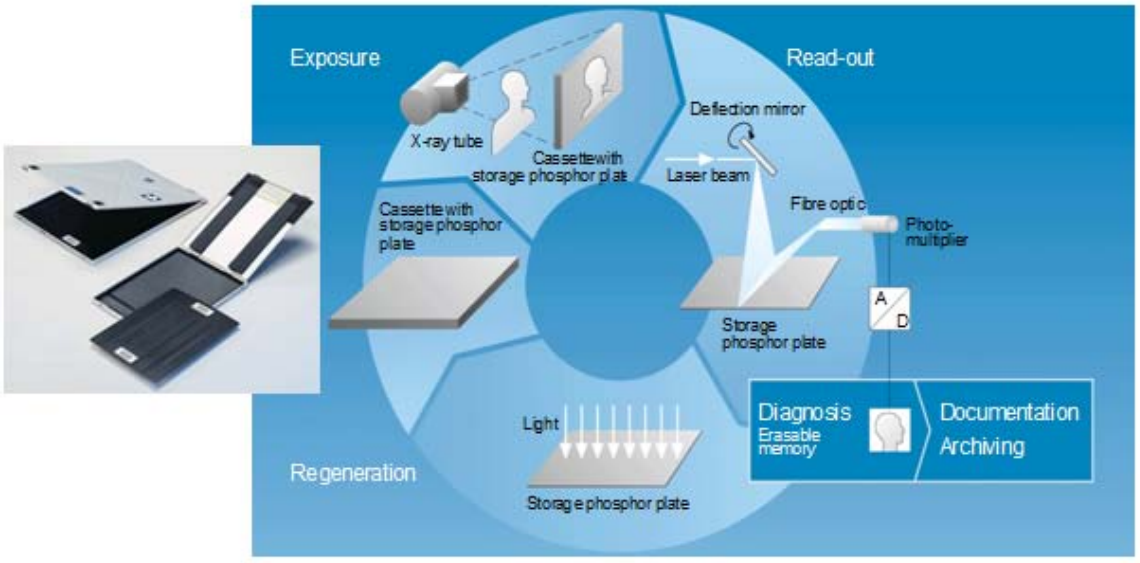

Figure 3 Cycle of re-use storage phosphor plate [5]

1.3 Image Qualities of Glass-ceramic storage phosphor

In Figure 4, the pictures were taken under several conditions to compare the image qualities of the traditional x-ray film vs. the glass-ceramic storage phosphor. Because the glass-ceramic storage phosphor can store the image in a digital format, the image can be easily corrected for brightness and contrast by analysis software. On the other hand, the image qualities of the traditional films cannot be improved easily.

The glass-ceramic storage phosphors with precipitated $BaCl_2$ nanoparticles have increased spatial resolution when compared to the BaFBr: Eu^{2+} Agfa MD-30 storage phosphor in Figure 5. The enhanced spatial resolution is attributed to the size of the $BaCl_2$ nanoparticles, which are much smaller than the size of crystallites embedded in the organic binder. The size of nanoparticles $BaCl_2$ can be observed with transmission electron microscopy. In Figure 5, both of the images were taken under the same condition. The parallel grids on the right image can be identified easily while the left image is blurred. The ceramic image plate outperforms the commercial product in spatial resolution.

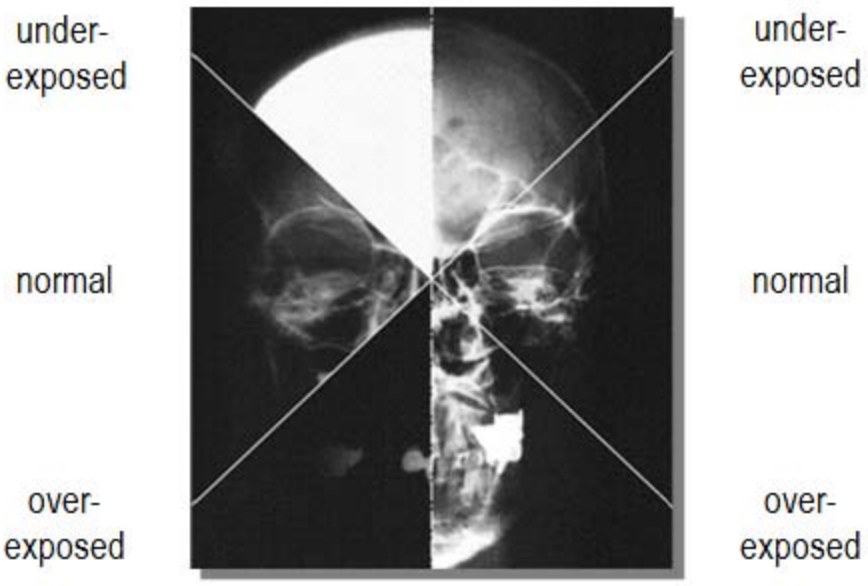

Figure 4 Comparison of images qualities of traditional film on the left vs. the glass ceramic storage phosphor on the right [4].

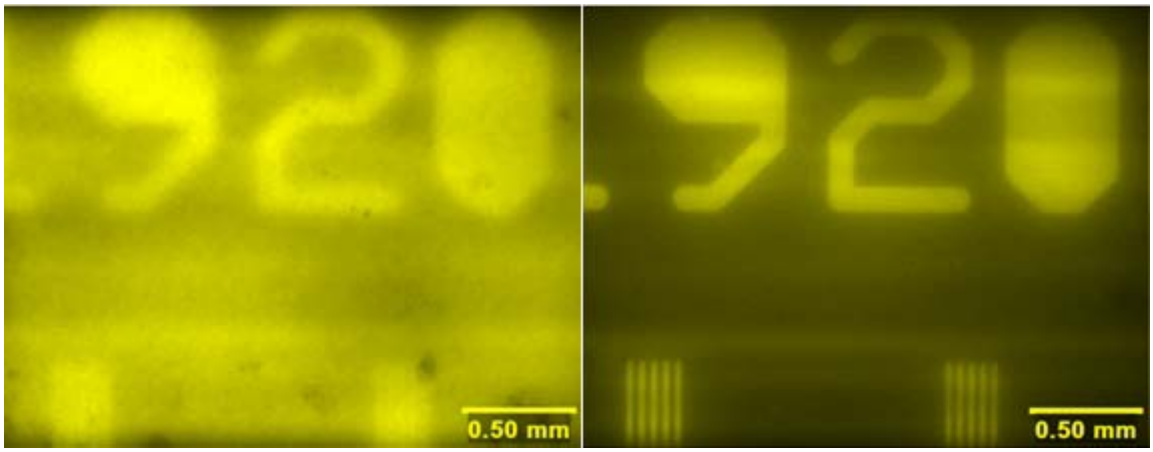

Figure 5 Comparison of image qualities of glass ceramic storage phosphor vs. Commercial product Agfa MD-30 [6]

CHAPTER II
EXPERIMENTAL DETAILS

ZBLAN glasses were produced in a glove box which is filled with argon gas. Characteristics of the glasses were studied by differential scanning calorimetry (DSC), X-ray diffraction (XRD), ion-chromatography, inductively coupled plasma spectroscopy, photoluminescence, and Mössbauer spectroscopy. Secondary ion mass spectrometry (SIMS) was used to further understand how the fluoride to oxygen ratio impacts the storage ability of the glasses. Transmission electron microscopy was used to study the growth of nanoparticles in the glass matrix.

2.1 Sample Preparation

Eu-doped fluorochlorozirconate glasses are based on a modified ZBLAN composition, listed in Table 1. Sealed chemical bottles (Aldrich Chemical Company, Milwaukee, WI) were opened inside the glove box (LABmaster SP, MBRUAN). The amount of oxygen and moisture in the glove box were monitored and maintained under 0.1 ppm. Samples were prepared by a two-step method. In the first melt, ZrF_4, NaF, AlF_3, LaF_3, and InF_3 were mixed in a platinum crucible inside the glove box. The crucible was covered with a lid to reduce chemical vaporization and placed inside a tube furnace (OTF 1220X, MTI Corporation) which is connected to the side of the glove box, as shown in Figure 7. The batches were melted according to the steps in Table 2. At the end of the fifth step, the platinum crucible was taken out of the tube furnace, and then $BaCl_2$, $EuCl_2$, and $EuCl_3$ were added for the second melt. At the end of the eighth step, the glass was then poured into a brass mold, which was pre-heated to 200°C. The melt in the pre-heated mold was then slowly cooled to room temperature over a time span of four hours. The two-step melting procedure has been shown to decrease the loss of chlorides in the glass and produce the desired phase transition. [7]

The glass samples were cut into pieces of about 1 cm × 1 cm × 1.6 mm (thickness) before they were annealed in a tube furnace filled with air to form $BaCl_2$ nanoparticles. The samples were annealed from 250°C to 300°C with 10°C steps. The annealing times were varied from 4, 5, 6 to 7 min for each annealing temperature to compare and study the optimal annealing temperature and time of each sample.

Figure 9 shows the first attempt to scale-up the glass-ceramic storage phosphor to 6.5 mm × 3.25 mm × 1.6 mm. It took more than one hour to anneal the large plate at 290°C to form $BaCl_2$ nanoparticles in the glass matrix. The glass-ceramic storage phosphor becomes translucent after annealing.

Table 1 Composition of the ZBLAN glasses for 2 mole % europium series and 5 mole % europium series.

Sample	ZrF_4	$BaCl_2$	NaF	AlF_3	LaF_3	InF_3	$EuCl_2$	$EuCl_3$
JJ 071	51.00	20.00	20.00	3.00	3.50	0.50	2.00	0.00
JJ 092	51.00	20.00	20.00	3.00	3.50	0.50	0.00	2.00
JJ 093	51.00	20.00	20.00	3.00	3.50	0.50	1.60	0.40
JJ 094	51.00	20.00	20.00	3.00	3.50	0.50	1.20	0.80
JJ 095	51.00	20.00	20.00	3.00	3.50	0.50	0.80	1.20
JJ 096	51.00	20.00	20.00	3.00	3.50	0.50	0.40	1.60
JJ 112	51.00	17.00	20.00	3.00	3.50	0.50	5.00	0.00
JJ 113	51.00	17.00	20.00	3.00	3.50	0.50	0.00	5.00
JJ 114	51.00	17.00	20.00	3.00	3.50	0.50	2.50	2.50

Table 2 Heating steps of the furnace

Step	Time/ min	Temperature / ℃
1	15	400
2	75	400
3	115	800
4	175	800
5	195	745
6	255	745
7	260	700
8	265	700
9	265	RT

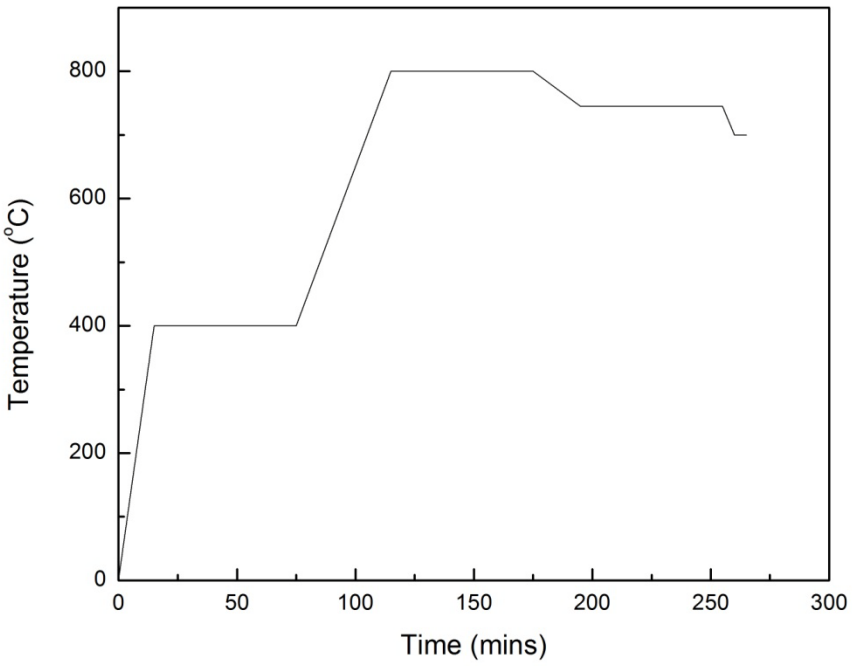

Figure 6 Graph heating steps of furnace

Figure 7 Glove box connected to the furnace on the left

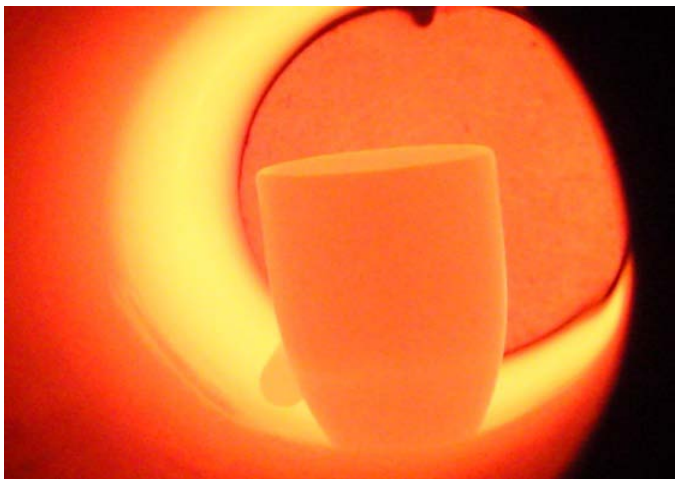

Figure 8 Crucible is heated inside the furnace

Figure 9 Before annealing ZBLAN glass sample on the left, the same sample after annealing at 290 °C.

2.2 Differential Scanning Calorimetry (DSC)

Differential scanning calorimetry was designed to have two heating plates, one is for heating the empty aluminum crucible and the other for heating crucible containing sample. The two crucibles are heated to the sample temperature, the different amount of heat required for each crucible are plotted as function of temperature. The glass transition temperature, crystallization temperature and melting temperature were measured using the DSC 200 ***F3*** *Maia*® (Netzsch) Differential Scanning Calorimeter with temperature range of room temperature to 600°C. The weight of the samples, crucibles and lids were recorded. A typical DSC measurement is performed with a constant heating rate of 10 K/min.

Figure 10 DSC 200 *F3 Maia*®, Differential Scanning Calorimeter [8]

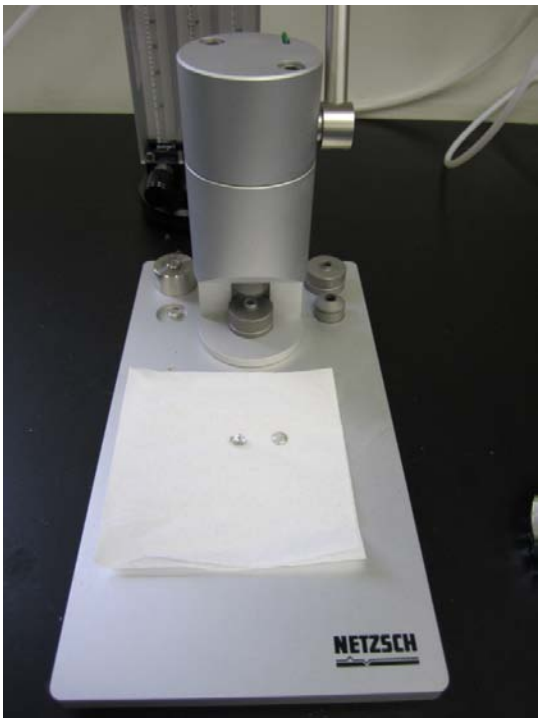

Figure 11 Crucible sealing press with exchangeable inserts and crucible

2.3 X-Ray Diffraction

X-ray diffraction (XRD) was performed on ZBLAN glasses to obtain structural information such as lattice structure, chemical composition. The experiment follows Bragg's Law. Waves scattered from the two Bragg planes in phase will create constructive and destructive interference. The interatomic spacing and distance between the lattice planes, ***d***, can be calculated using the Bragg equation.

$$\boldsymbol{n \cdot \lambda = 2 \cdot d \cdot \sin \theta}$$

The experiments were performed by the Philips X'Pert XRD instrument with an x-ray tube using a tungsten anode and Copper Kα target. The instrument was set to collect the counts from an angle of 20 degrees to 80 degrees, with step size 0.01 degrees and time per step, 4s. The total time for the measurement is around 12 hours. JADE 9.1 Software and Crystallography Database were used to analyze the lattice structure and chemical composition of the glasses.

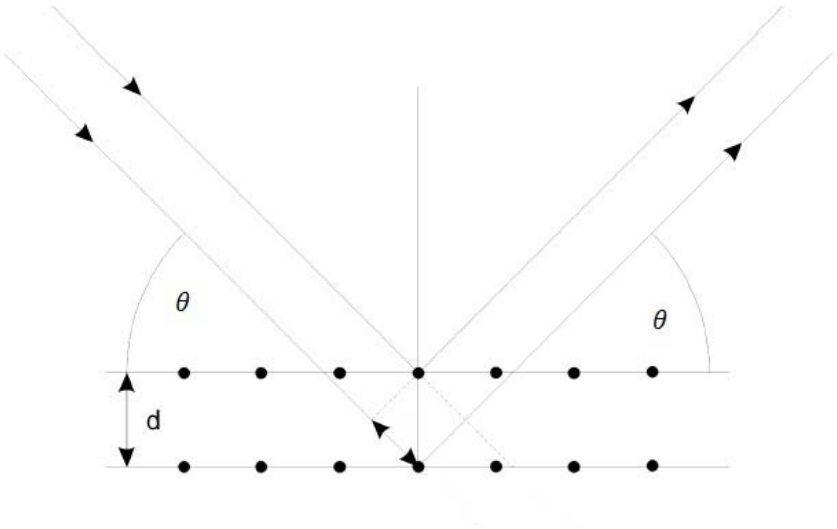

Figure 12 Bragg scattering from two successive planes.

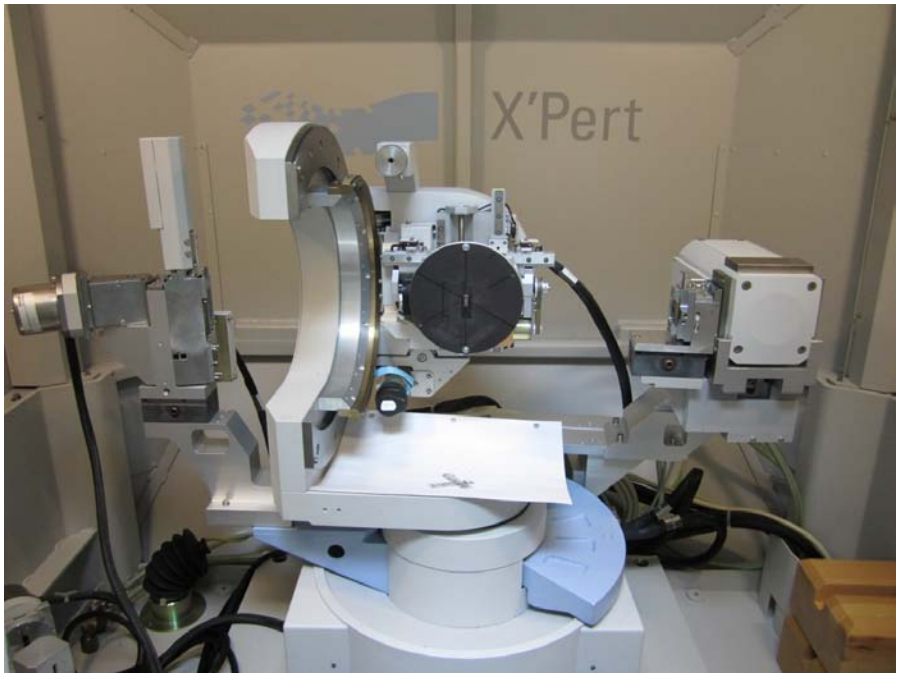

Figure 13 Philips X'Pert sample chamber

2.4 Secondary Ion Mass Spectroscopy

Secondary ion mass spectroscopy is one of the most sensitive techniques to detect impurities on the surface of bulk samples. In Figure 14, the surface of a sample is bombarded with heavy and high energy gallium ions. The beam sputters neutral and charged species from the surface; including atoms, clusters of atoms and molecular fragments. The pressure inside the sample chamber is maintained around 10^{-10} Torr to ensure a clean working environment. In our system, the quadrupole mass analyzer was used as a detector. The quadrupole mass analyzer is known to be more sensitive in a lower mass range.

The ratio of fluorine to oxygen in our ZBLAN glass samples were calculated from the areas under the curves of secondary ion mass spectroscopy. Samples were cut into plates with dimensions of 4 mm × 3 mm × 1.6 mm (thickness). The samples were cleaned using anhydrous ethanol and placed inside a vacuum oven for two hours to eliminate ambient moisture from the samples. Samples were prepared by two different methods to ascertain which method would yield the best results. In the first method, the samples were attached to the sample holder by carbon tape. The top surface of each of the samples was sputter coated with a thin layer of platinum to increase the ability of a specimen to conduct electricity and emit secondary ions. In the second method, a conducting collar was placed on top of uncoated samples. An electron beam is directed to the edge of the collar to offset the samples acquiring a positive charge due to Gallium ion bombardment.

The presence of oxygen and fluorine was measured on the surface and inside the samples after fracturing. Data was collected at five different areas per sample to obtain a more representative result.

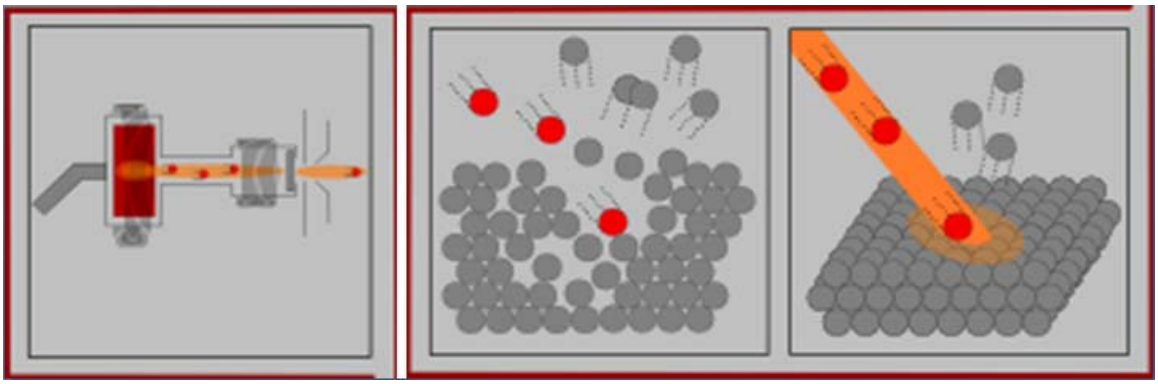

Figure 14 Gallium beam bombarding the sample surface [9]

Figure 15 SIMS samples holder

Figure 16 Secondary Ion Mass Spectroscopy

2.5 Phosphorimetry

Luminescence spectra of europium doped glasses were obtained using a PTI QM3 spectrofluorimeter (Birmingham, NJ). The data was analyzed using FeliX32 Version 1.2. Samples varied by different annealing conditions that included time of annealing and concomitant temperatures to further understand the optimal annealing condition. The higher annealing temperature and the longer annealing time are, the higher the degree of nucleation of $BaCl_2$ crystallites inside the glass matrix. As a result, more crystallites incorporate Eu^{2+} and hence increase the fluorescence intensity [10]. However, a higher annealing temperature and a longer annealing time also lead to a larger degree of crystal growth and result in bigger nanoparticles. It also leads to a decrease in spatial resolution of the ceramic-glass storage phosphor.

2.6 Ion Chromatography and Inductive Coupling Plasma

The process of preparing the sample requires a high heating temperature, therefore vaporization of chemical elements is inevitable. An Ion chromatography Dionex-ICS 100 and Dionex Automated Sampler (Sunnyvale, CA) were utilized to measure concentration of fluoride and chloride ions of as made samples. Inductively coupled plasma spectroscopy was performed using Perkin Elmer Plasma 40 Emission Spectrometer to determine the concentration of aluminum, barium, europium, indium, aluminum, lanthanum, sodium and zirconium.

Solutions for ion chromatography measurements were prepared following these steps. 5 g of anhydrous sodium carbonate and 0.5 g of powered ZBLAN glass sample were mixed inside a platinum crucible [11]. The crucible was placed in a furnace with a controlled argon gas atmosphere which was heated to 450°C for 30 min, and then the temperature was raised to 950°C in an inert argon atmosphere. The crucible was removed from the furnace after 30 min at 950°C and cooled down to room temperature.

Figure 17 Dionex Automated Sampler

The final product was ground into a fine power. The powder was digested in a one liter bottle of high-purity water and was stirred overnight in order to allow all the sodium fluoride to pass through the solution. The solution was filtered through a 1.5 μm membrane and diluted into different concentrations for the ion chromatography measurement. A Dionex chloride standard, 1000 g/l, and fluoride standard, 1000 g/l, were used for calibration.

2.7 Transmission Electron Microscopy

In-situ transmission electron microscopy was used to further understand the growth mechanism of nanoparticles inside the ZBLAN glass matrix under various heating conditions. The size of the nanoparticles was also analyzed.

Samples were prepared with great care and patience. A diamond saw was used to cut samples into small rectangles of 3 mm × 3 mm × 1.6 mm (thickness), which were then mounted on a metal block using an adhesive. The sample was mechanically polished to approximately 50 μm using successively finer grades of silicon carbide polishing paper, ending with hand polishing on 1200/2500P grade diamond polishing paper. The sample was removed from the metal block and glued on a 3 mm diameter SPI copper grid

to give mechanical stability. The sample and the grid were mounted on top of a block of glass and further thinned down to approximately 20 μm using the Original Dimpler 500i (VCR Group). The slowest rotation mode and the gentle force were used to dimple the sample. Knowing the refractive index of ZBLAN glass is around 1.5 [12], optical microscopy (Zeiss Axioskop) was used to determine the thickness of the samples. In the final step, the sample was removed from the glass block by soaking in acetone for 2 hours. Low temperature ion milling XLA 2000 (VCR Group) was used to mill down the sample until holes were created. The temperature was maintained at -50°C, with a voltage of 5000 to 6000 V and the current of gun A and B was approximately 2-3 mA. The sample was kept in the membrane box inside a nitrogen glove box until the TEM experiment was conducted.

Figure 18 South Bay Technology polishing tool.

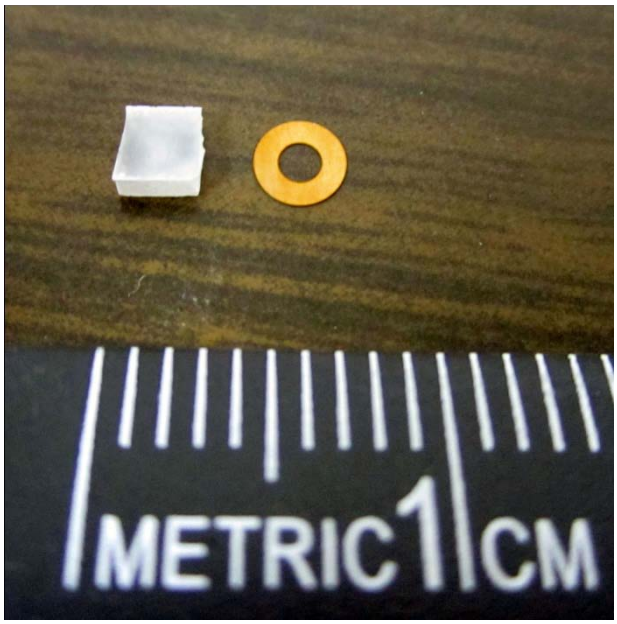

Figure 19 Rectangular sample and copper grid

Figure 20 Original Dimpler 500i [13]

2.8 Mössbauer Spectroscopy

The Mössbauer Effect was discovered in 1957 by R. Mössbauer. He discovered that a nucleus of Ir in a solid can sometimes emit and absorb gamma rays without recoil. Since his discovery, there have been a number of other isotopes exhibiting the same properties including Eu and Fe. This discovery was rewarded with the Nobel Prize in Physics in 1961. Mössbauer spectroscopy is generally not an appropriate technique for measuring the total concentration of a certain nuclide. However, the relative concentration of different chemical forms of the Mössbauer atom can frequently be obtained, such as the relative concentration of oxidation states for one element [14]. The relative concentration of Eu^{2+} to Eu^{3+} in ZBLAN glass samples was investigated using a SEE Co (Minneapolis, MN) Mössbauer Spectrometer (Figure 48, Figure 49). Mössbauer spectra were acquired by W302 software and analyzed by Mössbauer spectral analysis software which uses simple Lorentzian functions.

CHAPTER III

Results and Analysis

3.1 Differential Scanning Calorimetry

DSC was used to determine the temperature of the hexagonal to orthorhombic transitions of $BaCl_2$ crystallites in ZBLAN glasses. A typical DSC measurement of ZBLAN glass with a constant heating rate of 10 K/min is shown in Figure 21. The glass transition temperature, T_g, is correlated to the melting temperature, T_m, by the "two-thirds rule" $T_g/T_m = 2/3$ which applies for a large volume of liquid [15]. The crystallization of $BaCl_2$, T_{x1}, the crystallization of the glass matrix, T_{x2}, and the melting temperature T_m are identified by the intersection of two tangential lines which is also known as the onset method of the crystallization [16-18].

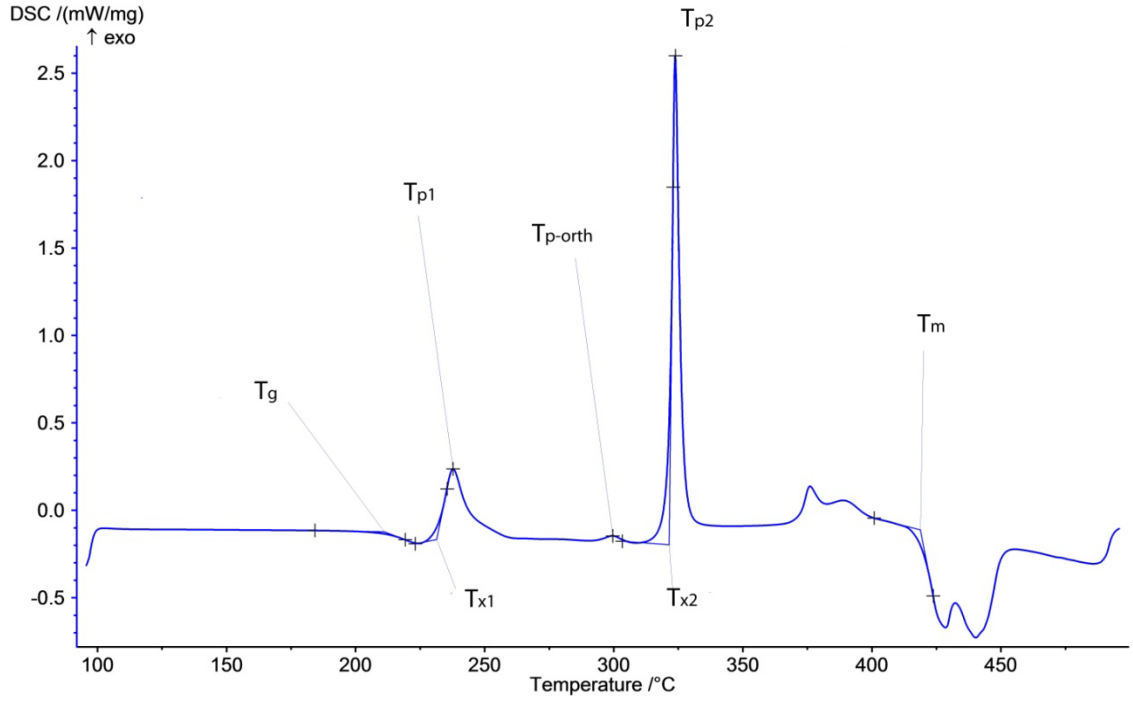

Figure 21 Plot of typical DSC data with the heating rate 10 K/min

The DSC data results are shown in Figure 22 and Table 3 for the europium 2 mole % series T_g is around 210 ± 5°C. In the europium 2 mole % series, higher Eu^{3+}-doping leads to an increase in the crystallization temperature of the second peak.

Figure 23 shows that for the europium 5 mole % series T_g is around 213 ± 2°C. In the europium 5 mole % series, the higher Eu^{2+}-doping, the higher the crystallization temperature (T_{x2}) and peak temperature of the second peak (T_{p2}) are.

The crystallization temperature of $BaCl_2$, T_{x1}, does not change much with the increasing of Eu^{2+} -doping. The second crystallization peak (T_{x2}) is associated with crystallization of the whole glass matrix.

Table 3, the orthorhombic peak of $BaCl_2$ ($T_{p\text{-}orth}$) is around 300 ± 10 °C for both the 2 mole % and 5 mole % europium doping series.

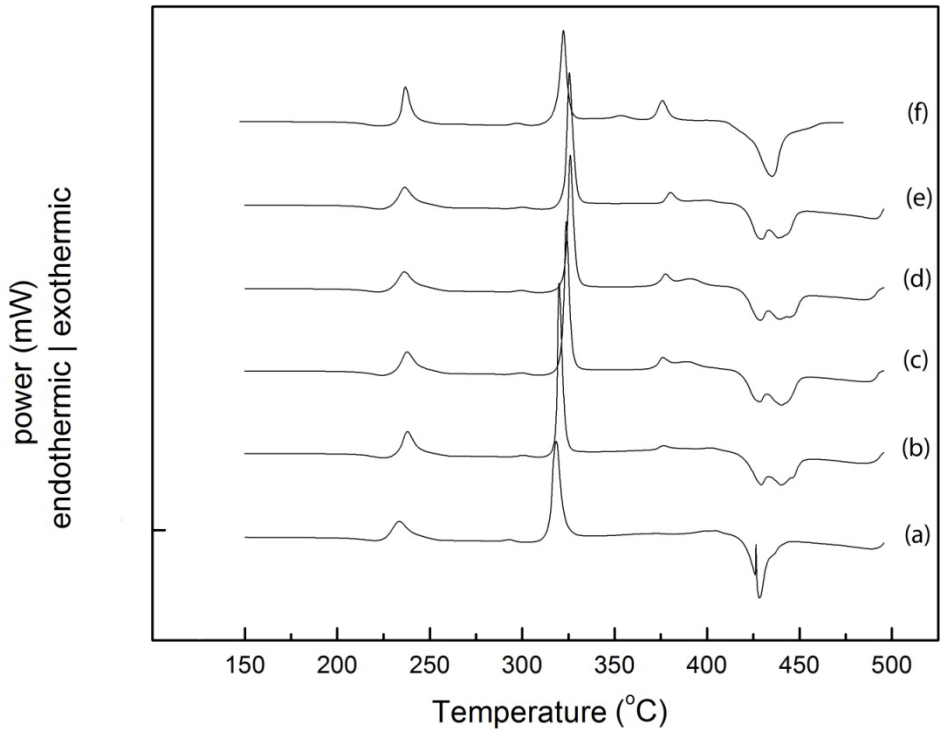

Figure 22 DSC graphs: the series of ZBLAN glass samples with 2 mole % of mixture $EuCl_2$ and $EuCl_3$ doping;(a) 2 mole % of $EuCl_2$ (b) 1.6 mole % of $EuCl_2$ and 0.4 mole % of $EuCl_3$ (c) 1.2 mole % of $EuCl_2$ and 0.8 mole % of $EuCl_3$ (d) 0.8 mole % of $EuCl_2$ and 1.2 mole % $EuCl_3$ (e) 0.4 mole %$EuCl_2$ and 1.6 mole % of $EuCl_3$ (f) 2 mole % of $EuCl_3$

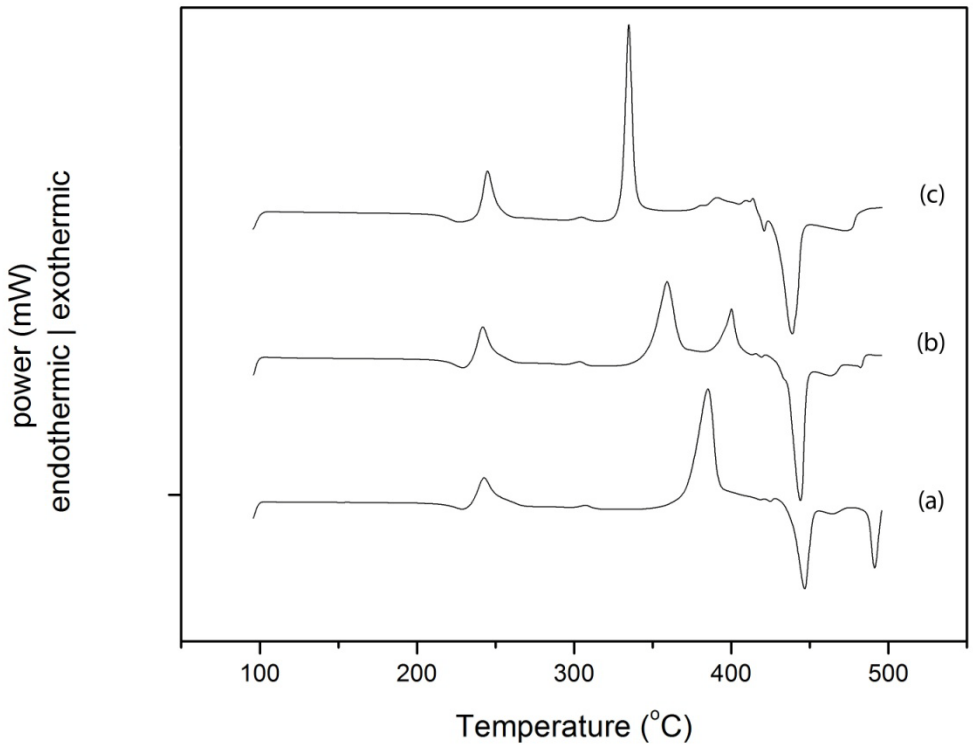

Figure 23 DSC graphs: the series of ZBLAN glass samples with 5 mole % of mixture $EuCl_2$ and $EuCl_3$ doping; ; (a) 5 mole % of $EuCl_2$ (b) 2.5 mole % of $EuCl_2$ and 2.5 mole % of $EuCl_3$ (c) 5 mole % of $EuCl_3$

Table 3 DSC data: glass transition, crystallization and peak temperature of 2 series 2 mole % and 5 mole % europium doping

Samples	T_g	T_{x1}	T_{p1}	$T_{p\text{-}orth}$	T_{x2}	T_{p2}	T_m	T_g/T_m
JJ 071	206.2	225.5	233.5	293.0	314.0	318.4	426.0	0.484
JJ 093	211.5	232.4	238.0	300.8	318.4	319.9	418.0	0.506
JJ 094	211.1	231.4	237.8	299.6	321.5	323.9	418.8	0.504
JJ 095	208.2	228.8	236.3	299.7	323.3	326.0	419.6	0.496
JJ 096	209.4	229.7	236.5	300.5	323.0	325.5	419.7	0.499
JJ 092	214.3	241.2	244.8	308.9	331.6	335.3	440.4	0.487
JJ 112	215.7	233.9	242.7	307.2	371.3	385.1	438.3	0.492
JJ 114	216.6	234.1	241.8	303.3	347.1	359.0	435.1	0.498
JJ 113	212.9	239.0	244.8	304.7	330.1	334.7	427.9	0.498

3.2 X-Ray Diffraction

The crystallographic structure of the nanoparticles is determined by x-ray diffraction. At a critical annealing temperature, the orthorhombic phase of $BaCl_2$ is formed inside the glass matrix. The storage phosphor effect was attributed to the orthorhombic phase of $BaCl_2$ [1, 3]. X-ray diffraction verifies the existence of the hexagonal and orthorhombic phase of $BaCl_2$ in ZBLAN glasses matrix after annealing.

Figure 24 shows the x-ray diffraction patterns of 5 samples with different composition of $EuCl_2$ and $EuCl_3$ which were annealed at 300°C for 5 min. The XRD line pattern of the crystal $BaCl_2$ hexagonal phase (PDF # 45-1313) is shown at the top of the graph. The XRD line pattern of the crystal $BaCl_2$ orthorhombic phase (PDF # 24-0094) is at the bottom of the graph. The software analysis Materials Dada Jade 9.1 was used to find and match the structural phase for the spectra. The $BaCl_2$ orthorhombic phase was the best possible match for the spectra.

Figure 25 shows the x-ray diffraction of sample JJ 092 at 5 different annealing temperatures from 250 °C to 290 °C in order to find the critical temperatures where most of the $BaCl_2$ nanoparticles convert from the hexagonal to orthorhombic phase. The higher the annealing temperature, the more $BaCl_2$ transforms from the hexagonal phase into the orthorhombic phase.

The XRD results show that the higher the annealing temperature, the more $BaCl_2$ nanoparticles in hexagonal phase convert into orthorhombic phase. The results are consistent with the DSC analysis.

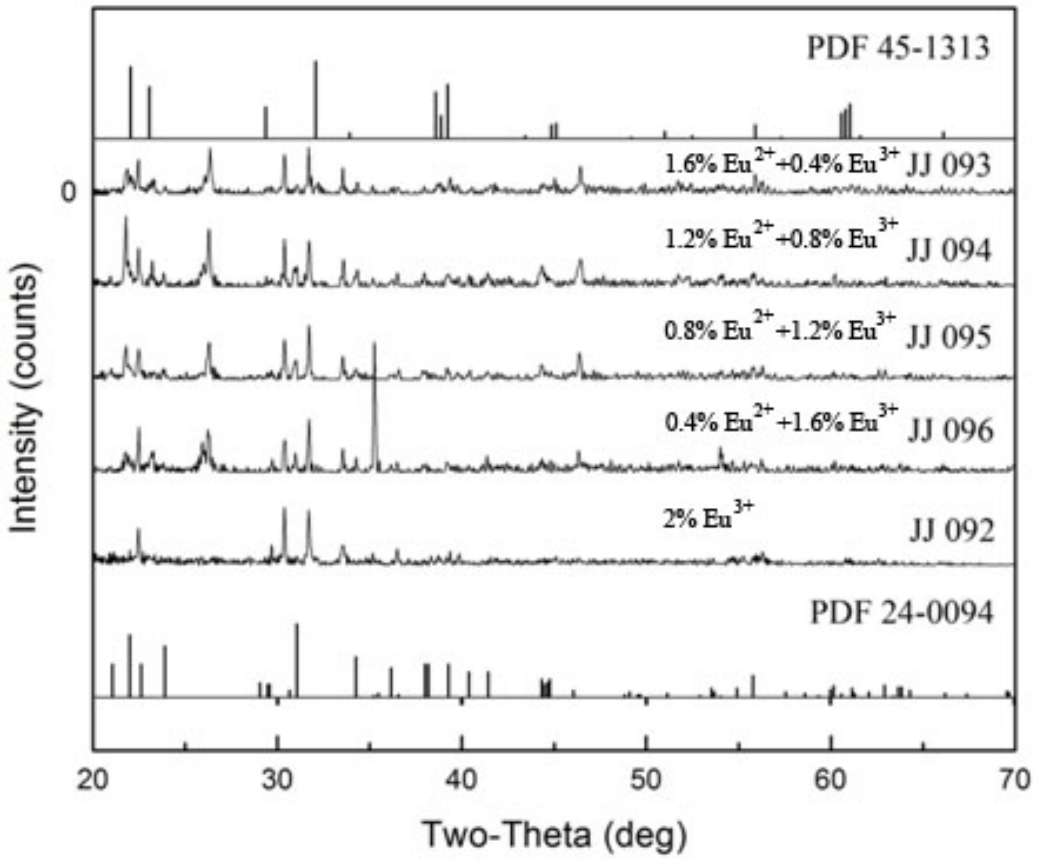

Figure 24 X-ray diffraction patterns of 5 different samples at 300°C.

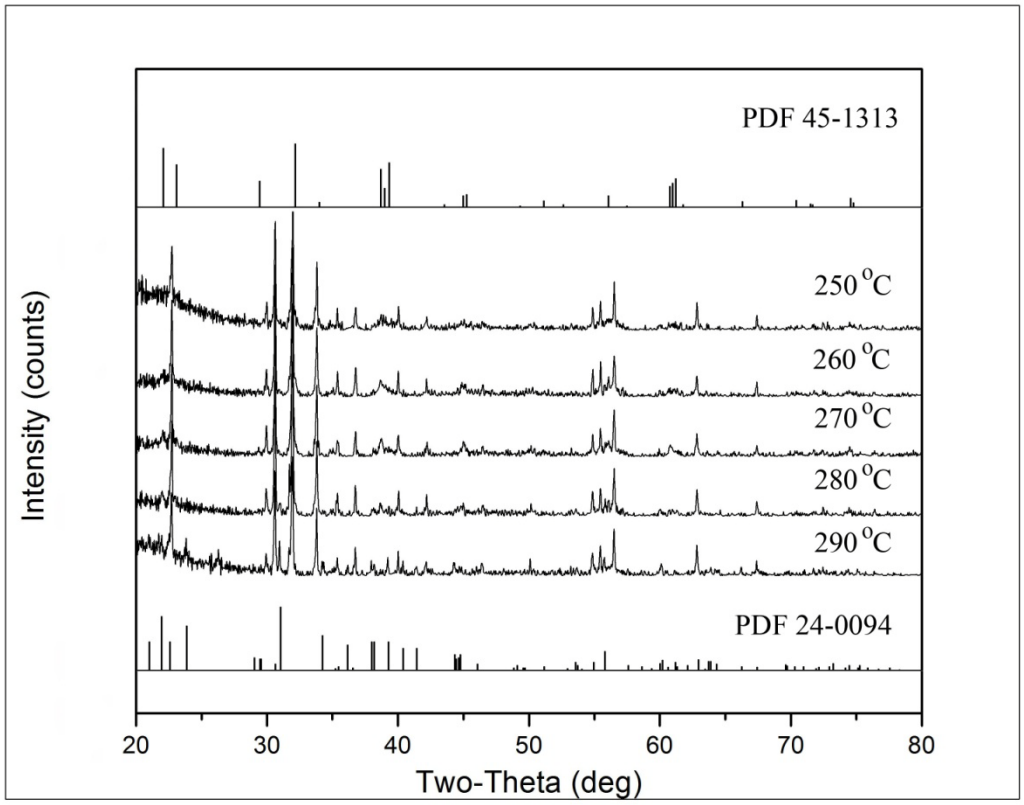

Figure 25 X-ray diffraction of sample JJ 092 with 2% of $EuCl_3$ annealing from 250 °C to 290 °C for 5 min

3.3 Secondary Ion Mass Spectroscopy

The presence of oxygen may oxidize Eu^{2+} and reduce the performance of ZBLAN glass as an image plate. Secondary ion mass spectroscopy was utilized to estimate the presence of oxygen and calculate the ratio of fluorine to oxygen content in the glass samples. Samples were selected from four different groups. Sample JJ083 was prepared at the University of Tennessee Space Institute using a glove box which was filled with argon gas. The amount of oxygen and moisture in the glove box atmosphere was maintained below 0.1 ppm. Sample ZBLAN 76 was prepared in Germany using a glove box that was filled with nitrogen gas. Sample Pour 5 was prepared by Dr. Richard Weber from Illinois using a glove box which is filled with nitrogen gas. Sample N04.02.22 was prepared in Australia and was exposed to oxygen gas for 15 minutes to reduce the black precipitates in the sample and improve the quality of the glass.

The approach of using uncoated samples with a conducting collar gave better results [19, 20]. Each sample was scanned in negative ion mode from 2 to 50 amu with step size 0.1 and dwell time 0.05 s. Figure 26 shows the distribution of fluoride content both on the surface and inside sample JJ083. The brighter region (inside the sample), where the surface layer was scraped off, shows relatively more fluoride than oxygen. Figure 27 shows a strong peak at 16 amu (oxygen), 19 amu (fluorine) and 35.5 amu (chlorine) for the mass spectrum of the surface of the sample. This shows there is more oxygen on the surface of the sample than inside the sample. The ratio of fluorine to oxygen was calculated by using the ratio of the area under of the curves. The intensity of the peak for the surface is not as strong as the intensity for the peak inside. These reasons were attribute to the contact of the glass surface to the brass mold during the cooling process. Analogous results are shown in Figure 28, Figure 30, Figure 32 and Figure 29, Figure 31, Figure 33.

Table 4 shows that the results are consistent with sample preparation. Sample JJ083 shows the least amount of oxygen due to the procedure in which the sample was

prepared in a highly monitored atmosphere with less than 0.1 ppm of oxygen and moisture. Sample N04.02.22 shows the most oxygen due to the introduction of oxygen flow during synthesis to improve the quality of the glass. Sample ZBLAN 76 and Pour 5 show higher oxygen due to the nitrogen gas environment and a less sophisticated glove box. Most of the oxygen of those samples concentrates on the surface; it is attributed to the contact of the sample on the molds. Also, ZBLAN glasses are somewhat hydrophilic and absorb ambient moisture.

Table 4 Fluorine to oxygen ratio on the surface and inside 4 glass samples

Ratio F/O	JJ 083	ZBLAN 76	Pour 5	N04.02.22
Surface	2	7	6	6
Inside	18	18	13	10

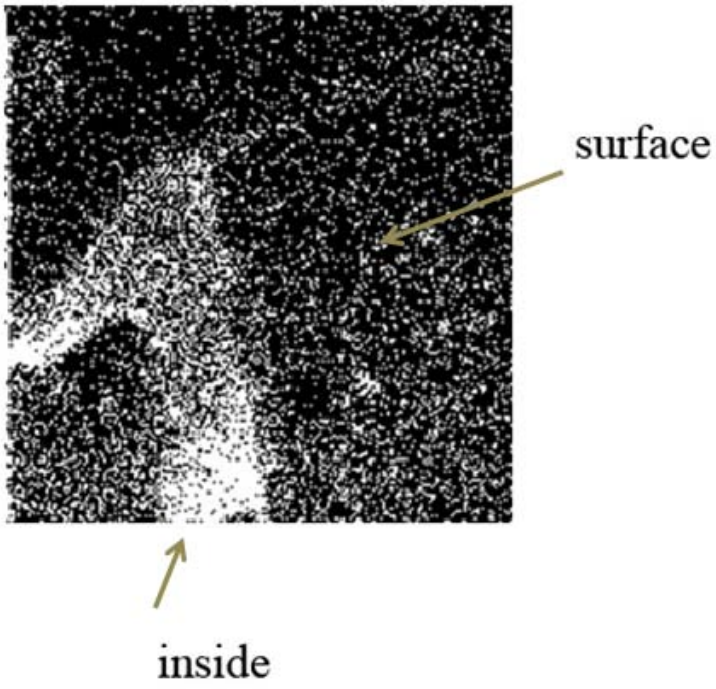

Figure 26 Fluorine distribution both inside and on the surface of sample JJ083

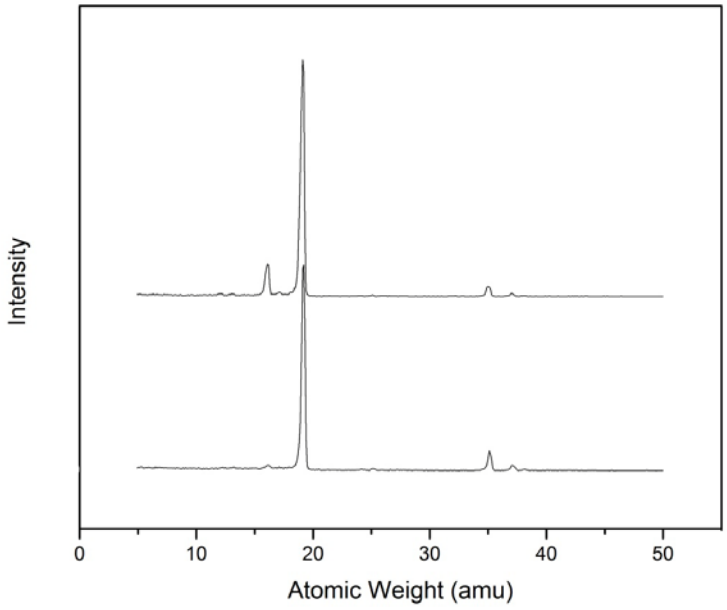

Figure 27 SIMS spectra of sample JJ083 for both surface (top) and inside (bottom)

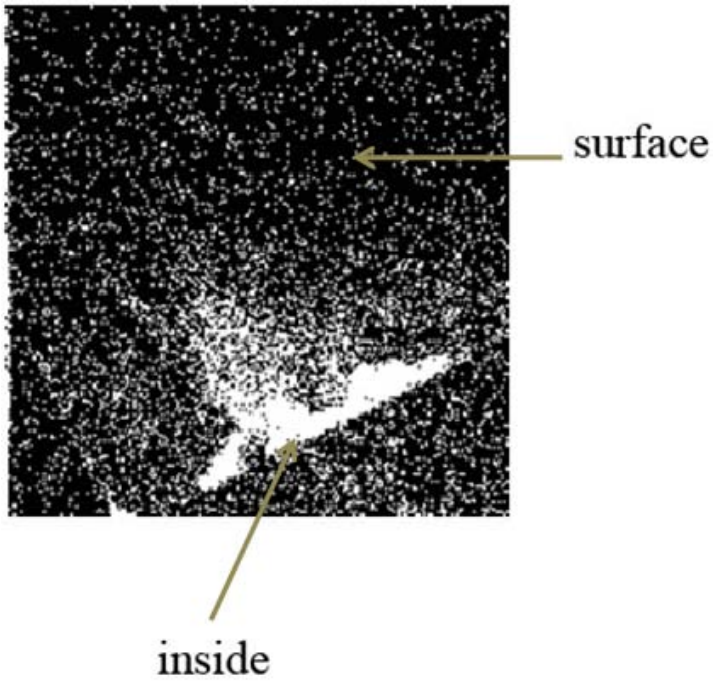

Figure 28 Fluorine distribution both inside and on the surface of sample ZBLAN 76

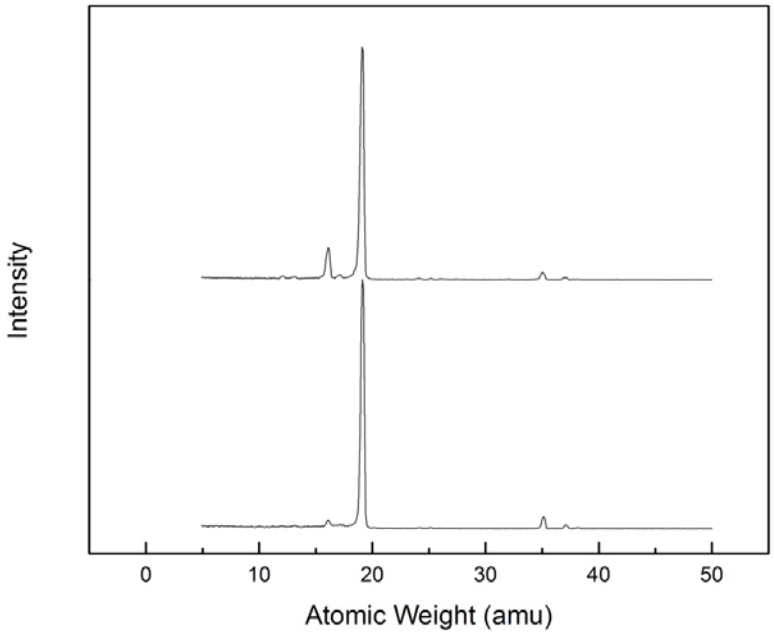

Figure 29 SIMS spectra of sample ZBLAN 76 for both surface (top) and inside (bottom)

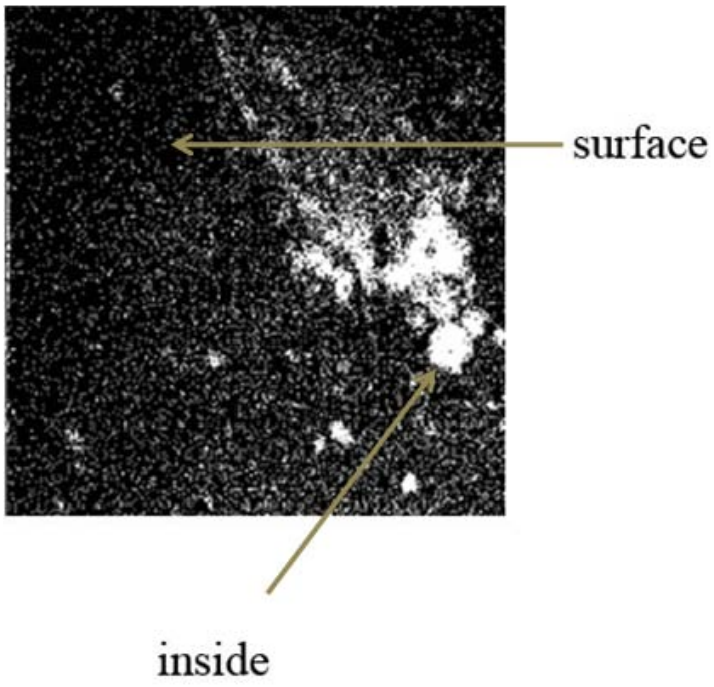

Figure 30 Fluorine distribution for both inside and on the surface of sample Pour 5

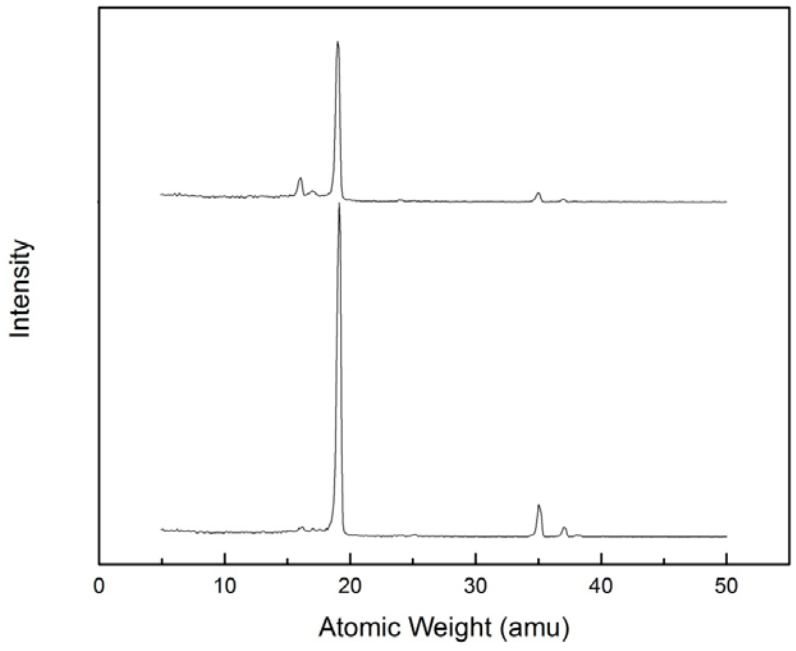

Figure 31 SIMS spectra of sample Pour 5 for both surface (top) and inside (bottom)

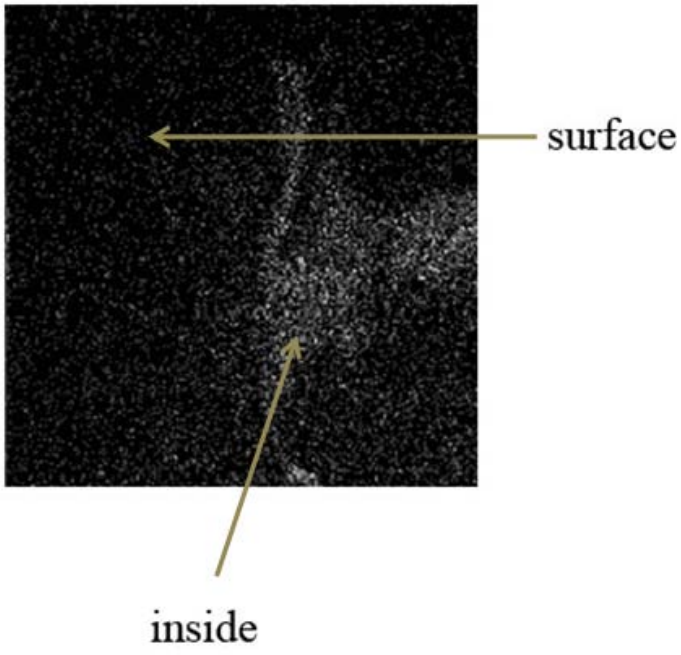

Figure 32 Fluorine distribution for both inside and on the surface of sample N04.02.22

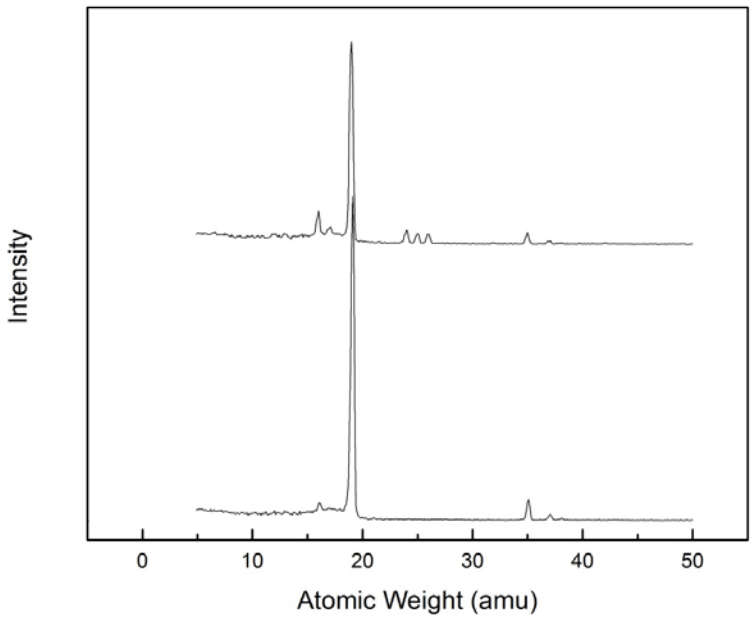

Figure 33 SIMS spectra of sample N04.02.22 for both surface (top) and inside (bottom)

3.4 Phosphorimetry

Annealed ZBLAN glass samples were tested under UV light as shown in Figure 34. This study helps to determine the performance of the glass as an imaging plate. The samples on the left are annealed at 300°C and glow violet as they are mostly ceramics. The samples on the right are annealed at lower temperature, 280°C, and glow blue. The samples on the right still look transparent.

Figure 35 shows photoluminescence of sample JJ 093 prepared with 1.6 mole % $EuCl_2$ and 0.4 mole % $EuCl_3$ doped fluorochlorozirconate based glass excited at 285 nm. The peak around ~ 410 nm is shifted to around ~ 400 nm when the annealing temperature is increased. This shift is attributed to the transformation of a hexagonal phase of $BaCl_2$ into an orthorhombic phase of $BaCl_2$ [16, 21]. The peak around ~ 470 nm is attributed to the mixture of hexagonal and orthorhombic phases [22, 23]. The intensity of the peak around ~ 400 nm increased when the annealing temperature is increased. The same effect is also observed with sample JJ094, JJ095, and JJ096, which are shown in Figure 36- 38

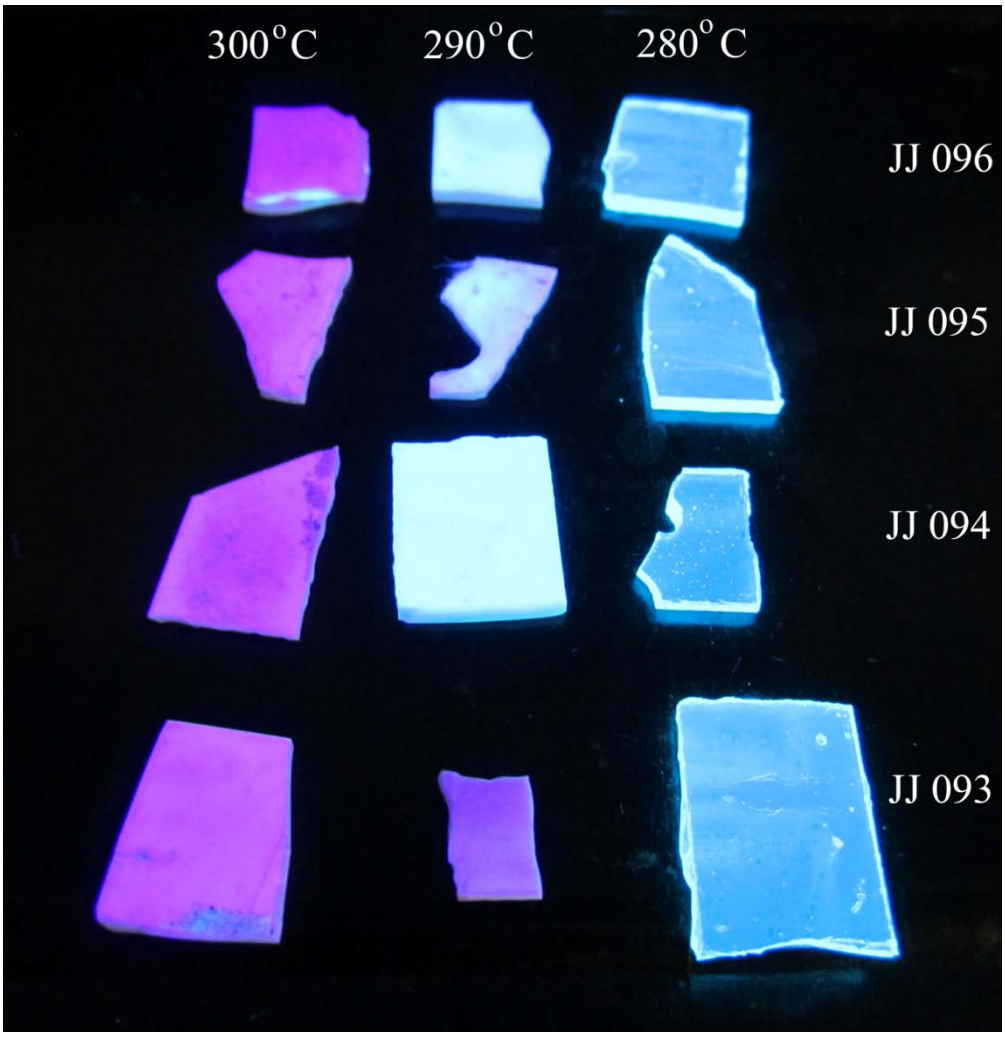

Figure 34 Photoluminescence test under UV light on ZBLAN glass sample doped with 2 % Eu^{2+} after annealing at different temperatures for 5 min.

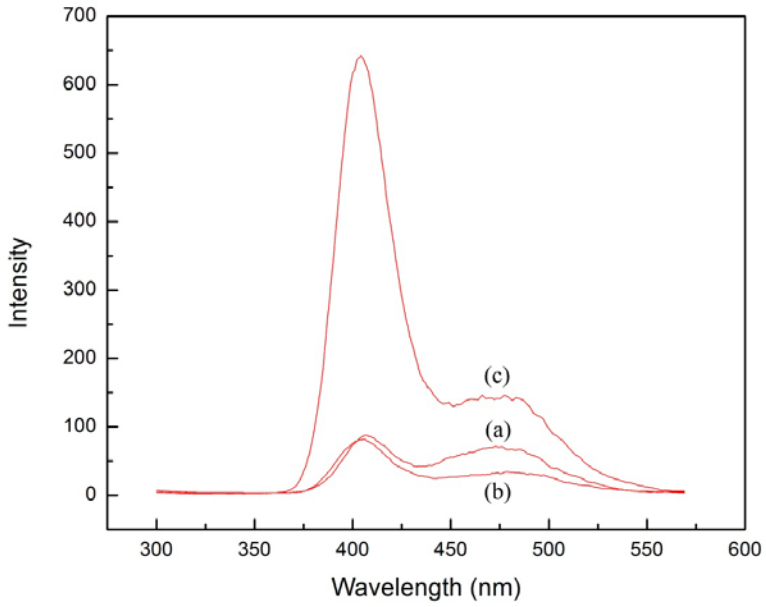

Figure 35 Photoluminescence spectroscopy of sample JJ 093 (a), (b) and (c) annealed at 280°C, 290°C, and 300°C respectively for 5 min.

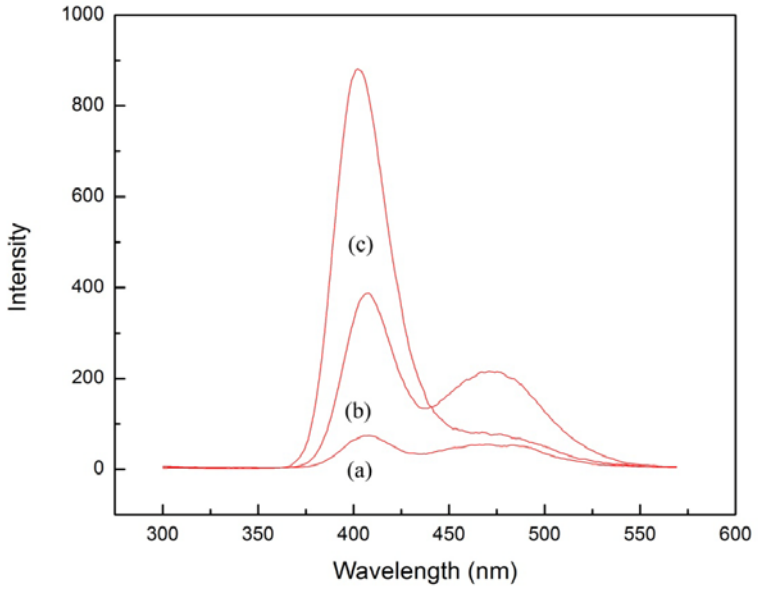

Figure 36 Photoluminescence spectroscopy of sample JJ 094 (a), (b) and (c) annealed at 280°C, 290°C, and 300°C respectively for 5 min.

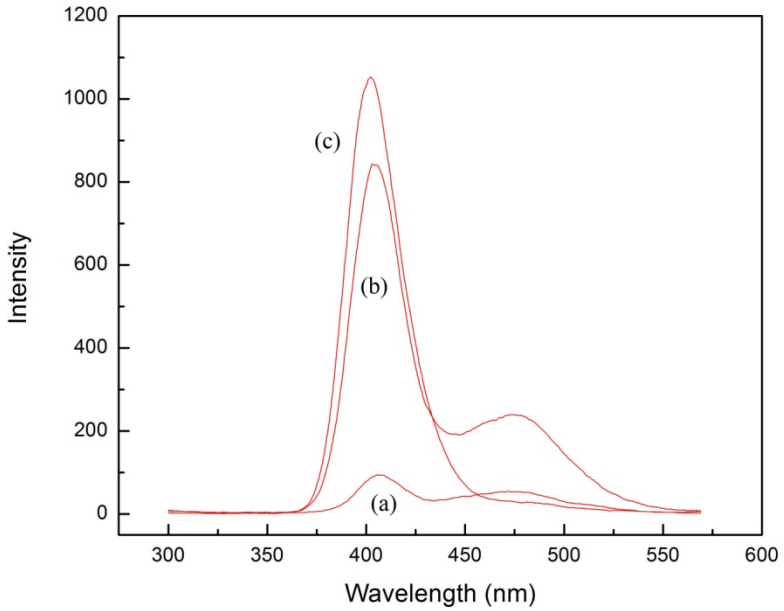

Figure 37 Photoluminescence spectroscopy of sample JJ 095 (a), (b) and (c) annealed at 280°C, 290°C, and 300°C respectively for 5 min.

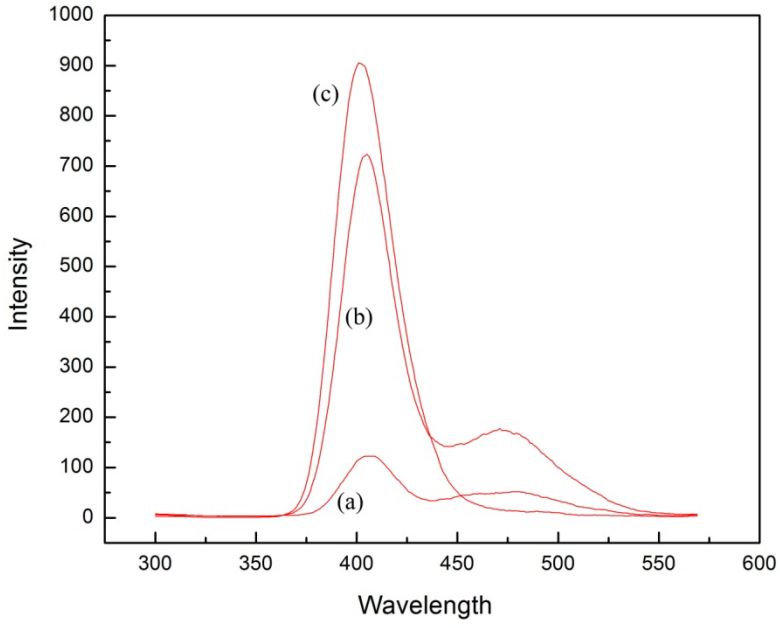

Figure 38 Photoluminescence spectroscopy of sample JJ 096 (a), (b) and (c) annealed at 280°C, 290°C, and 300°C respectively for 5 min.

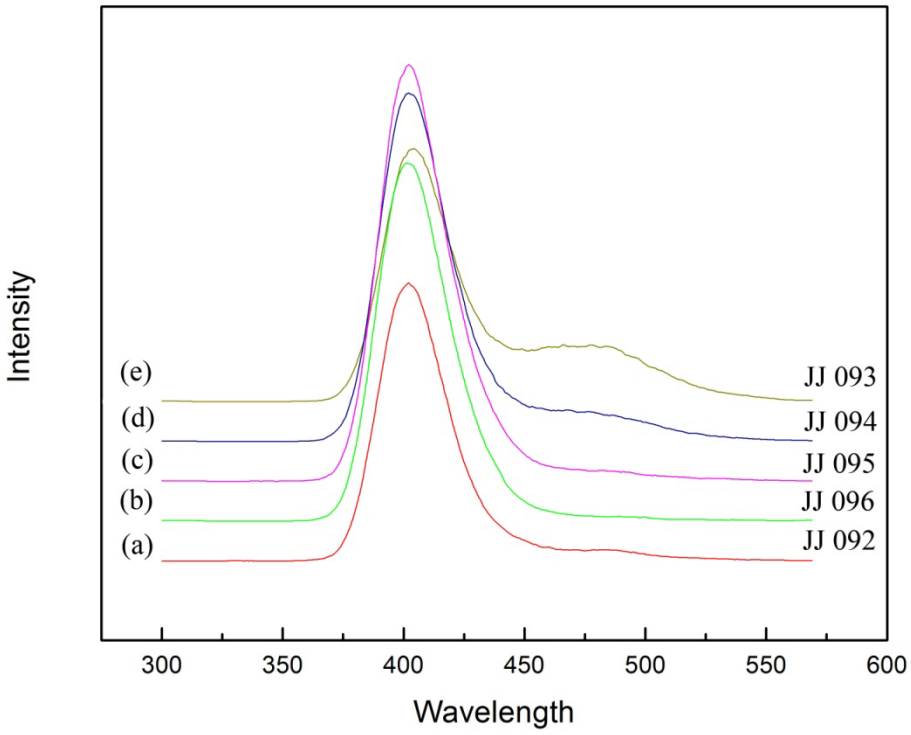

Figure 39 Photoluminescence spectroscopy of samples JJ092, JJ093, JJ094, JJ095, and JJ096, annealed at 300 °C for 5 min.

Figure 39 shows the comparison of photoluminescence for 5 different samples. The intensity of the peak around ~ 400 nm strongly depends on the annealing time and amount of Eu^{2+} in the samples. The peak around ~ 470 nm diminishes when the annealing temperature reaches 300 °C. That is explained by the hexagonal phase transforming into the orthorhombic phase at a high enough temperature. The five samples have different ratios of Eu^{2+} and Eu^{3+} but they do not show a difference in intensity for the fluorescence. The conclusion is that part of the Eu^{3+} reduces to Eu^{2+}. Even a low concentration of Eu^{2+} can give a high fluorescence intensity.

3.5 Ion Chromatography – Inductive Coupling Plasma

During the sample preparation process, the crucible was heated to high temperatures. Vaporization of the chemical elements is inevitable. Ion chromatography and inductively coupled plasma (ICP) spectroscopy were used to determine the weight loss of each element. The concentration of aluminum, barium, europium, indium, aluminum, lanthanum, sodium and zirconium were determined by ICP atomic emission spectrometry. The concentration found in the sample was compared with the expected values from Table 1. This comparison helps to detect whether any component is partially volatilized during manufacturing [11]. Furthermore, the uniformity of the glass can be evaluated by measuring different parts of the sample. Tables 5- 8 shows the cationic concentration in the samples JJ 093, JJ 094, JJ 095 and JJ096 that were measured using ICP, respectively. The mole percentage was found to be very close to the expected value. The weight loss of cations is very small.

Table 5 Concentrations of aluminum, barium, europium, indium, aluminum, lanthanum, sodium and zirconium of in ZBLAN glass sample JJ093

Element	Found (mg/g)	Found (millimole/gram)	Found (moles %)	Expected (moles %)
Al	4.134	0.15	2.3	3.0
Ba	198.65	1.45	21.7	20.0
Eu	23.595	0.16	2.3	2.0
In	0.5023	0.00	0.1	0.5
La	35.845	0.26	3.9	3.5
Na	34.97	1.52	22.8	20.0
Zr	284.5	3.12	46.8	51.0
		6.66	100.0	100.0

Table 6 Concentrations of aluminum, barium, europium, indium, aluminum, lanthanum, sodium and zirconium of in ZBLAN glass sample JJ094

Element	Found (mg/g)	Found (millimole/gram)	Found (moles %)	Expected (moles %)
Al	3.985	0.15	2.2	3.0
Ba	196.9	1.43	21.8	20.0
Eu	22.53	0.15	2.3	2.0
In	0.5102	0.00	0.1	0.5
La	35.28	0.25	3.9	3.5
Na	34.555	1.50	22.9	20.0
Zr	280.75	3.08	46.9	51.0
		6.57	100.0	100.0

Table 7 Concentrations of aluminum, barium, europium, indium, aluminum, lanthanum, sodium and zirconium of in ZBLAN glass sample JJ095

Element	Found (mg/g)	Found (millimole/gram)	Found (moles %)	Expected (moles %)
Al	3.996	0.15	2.2	3.0
Ba	197.5	1.44	21.8	20.0
Eu	22.745	0.15	2.3	2.0
In	0.4711	0.00	0.1	0.5
La	35.34	0.25	3.9	3.5
Na	34.67	1.51	22.9	20.0
Zr	282.5	3.10	46.9	51.0
		6.60	100.0	100.0

Table 8 Concentrations of aluminum, barium, europium, indium, aluminum, lanthanum, sodium and zirconium of in ZBLAN glass sample JJ096

Element	Found (mg/g)	Found (millimole/gram)	Found (moles %)	Expected (moles %)
Al	4.735	0.18	2.7	3.0
Ba	195.1	1.42	21.7	20.0
Eu	22.54	0.15	2.3	2.0
In	0.613	0.01	0.1	0.5
La	35.24	0.25	3.9	3.5
Na	34.53	1.50	22.9	20.0
Zr	278.85	3.06	46.6	51.0
		6.56	100.0	100.0

Figure 40 shows a typical graph of an ion chromatography measurement for anionic concentrations of fluorine and chlorine. The expected value for fluorine and chlorine were calculated based on the Table 1. Figure 40 shows a typical graph of ion chromatography measurement for concentrations of fluoride and chloride. The concentrations of fluorine and chlorine were measured using ion chromatography and compared to expected values. For a typical ZBLAN glass sample, the weight loss of fluorine is between 3-5 %, and the same for chlorine.

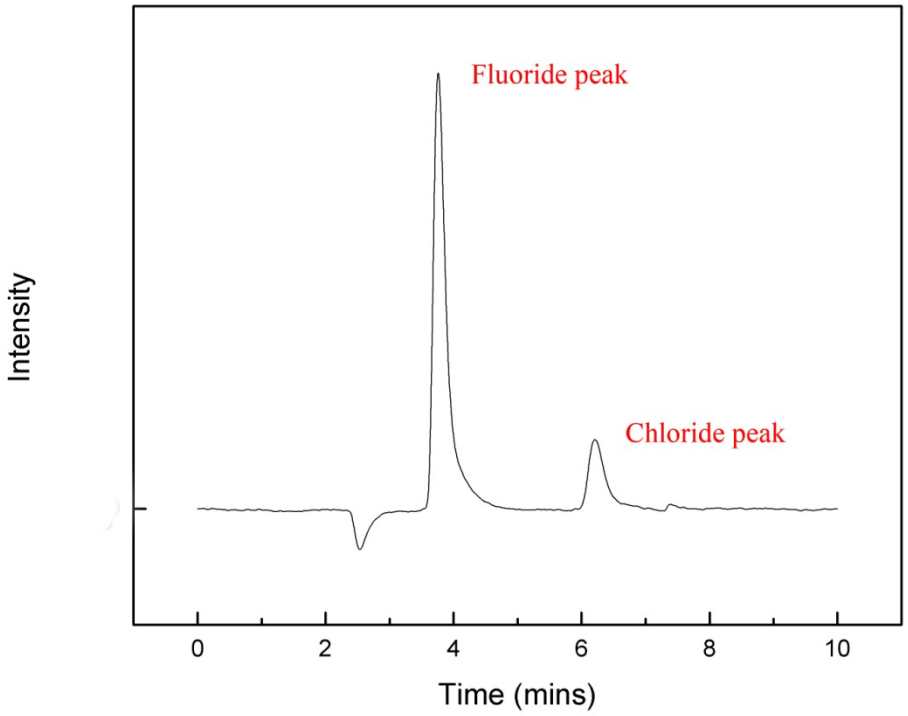

Figure 40 A typical graph of an ion chromatography measurement for concentrations of fluoride and chloride.

3.6 Transmission Electron Microscopy

Transmission electron microscopy was used to observe the formation and the propagation of $BaCl_2$ nanoparticles under various heating conditions. The results were consistent with other techniques.

During subsequent ion milling, the amorphous matrix may undergo partial crystallization (phase transition). For this reason, special precautions were taken to prevent crystallization during the ion milling. Figure 41 shows how the relative uniform contrast indicates that the sample is in amorphous state before the in situ experiment. The detailed formation of the nanostructure of $BaCl_2$ in the glass matrix was examined using high-resolution transmission electron microscopy.

The sample was slowly heated from room temperature to 300 °C to observe the $BaCl_2$ nanoparticles formation. It was found that the nanoparticles start to form when the annealing temperature is around 250-260 °C which is in agreement with the DSC and XRD study. The crystallization propagates to larger areas when the annealing temperature increases which corresponds to higher photoluminescence intensity. As a result, larger $BaCl_2$ nanoparticles are formed. Figure 42 shows small crystal areas inside the white square box, which were observed under high-resolution TEM. Figure 43 shows sample N05.02.41 after annealing and the formation of a crystal area of ~500 nm.

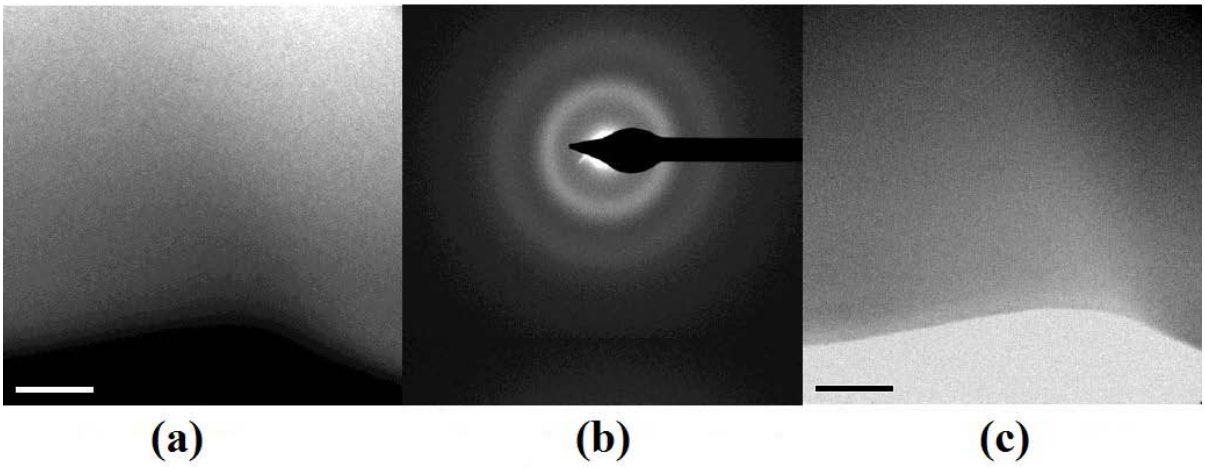

Figure 41 (a) dark field image, (b) amorphous diffraction rings, and (c) bright field image of ZBLAN glass sample JJ 094.

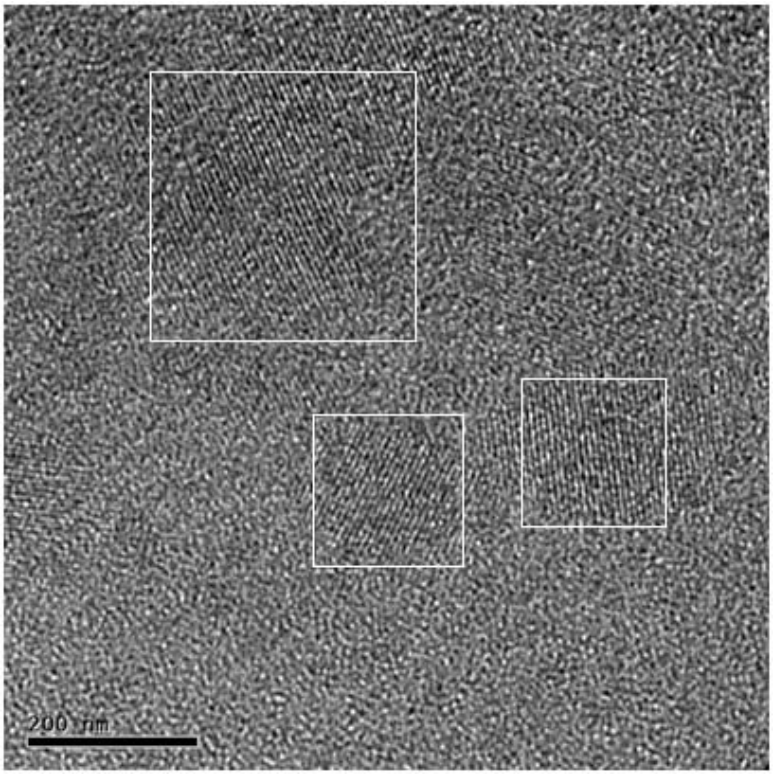

Figure 42 High resolution image of ZBLAN JJ 094 after heat treatment

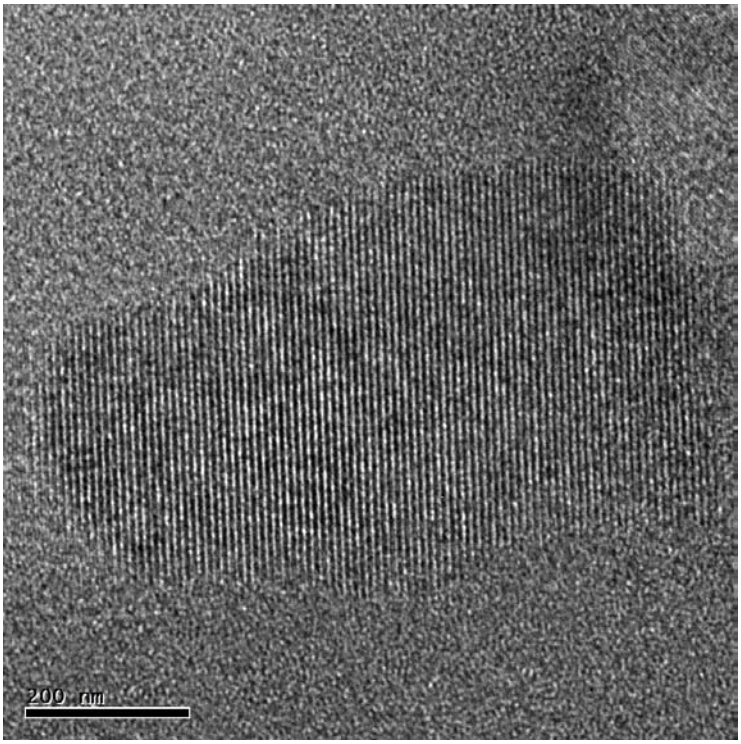

Figure 43 High resolution image of ZBLAN N05.02.41 after heat treatment

3.7 Mössbauer Spectroscopy

Eu^{3+} is the stable oxidation state of europium. Eu^{2+} easily oxidizes to Eu^{3+} in the presence of moisture or oxygen. $EuCl_2$ and EuF_2 are important in the formation of glass-ceramic storage phosphors, but they are around twenty times more expensive than $EuCl_3$ and EuF_3. Mössbauer spectroscopy was able to demonstrate the ability of producing $EuCl_2$ from $EuCl_3$ in the laboratory environment.

Sealed bottles of 99.9% purity $EuCl_3$ (Aldrich Chemical Company, Milwaukee, WI) were opened inside the glove box (LABmaster SP, MBRUAN). Europium (III) chloride, when heated under argon gas at 750 °C for one hour, allowed the following reaction to occur [24]

$$EuCl_3(s) \xrightarrow{\text{Heat}} EuCl_2(s) + \frac{1}{2}Cl_2(g)$$

The melting point of $EuCl_3$ is 625 °C [25, 26] which is lower than the heating temperature. After heating $EuCl_3$, the final product changed from a white to dark grey color. Eu^{3+} and Eu^{2+} are known to have an isomer shift around 0 mm/s and -13 mm/s, respectively [27]. The relative area under the peaks represents the relative presence of Eu^{2+} and Eu^{3+} in samples. The longer the samples were exposed to air, the more Eu^{2+} oxidized to Eu^{3+}. Figure 44 shows the increasing concentration of Eu^{3+} and the decreasing concentration of Eu^{2+} in the sample over time. The lower the concentration of Eu^{2+}, the weaker the interaction between Eu^{2+}-Eu^{2+} is leading to an increased linewidth of Eu^{2+} over time.

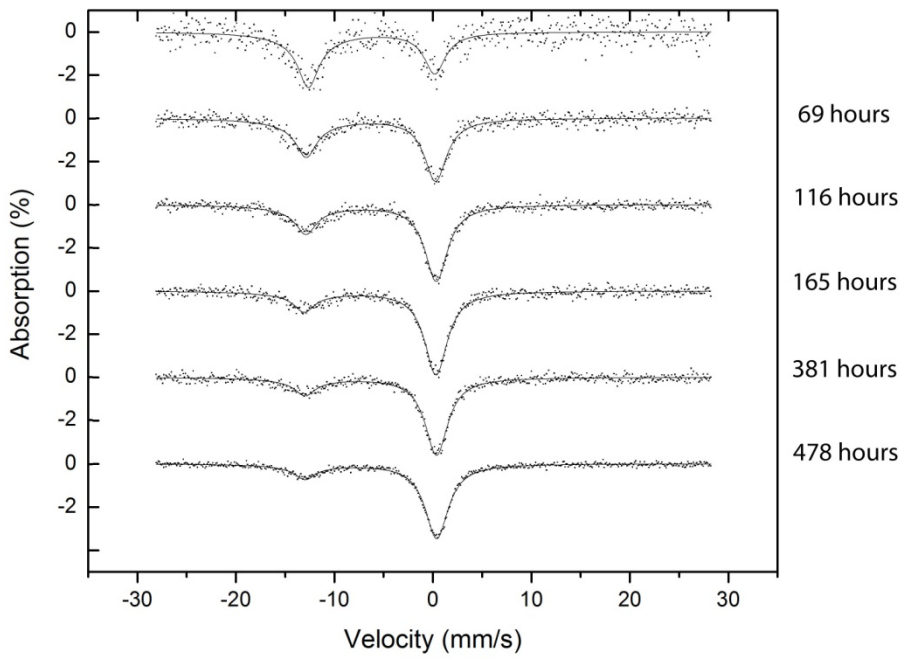

Figure 44 Mössbauer spectra of $EuCl_3$ heated at 700 °C for an hour as a function of time.

Figure 45 shows the decrease in concentration of Eu^{2+} in heated $EuCl_3$ fine powder. The oxidation rate of Eu^{2+} follows a negative exponential curve $y = 64.3 \exp\left(-\frac{t}{6.9}\right)$, which is consistent with our hypothesis that the less Eu^{2+} on a surface layer and the thicker the oxide layer is the longer and the more difficult it is for moisture and oxygen to penetrate the samples. Moreover, the fitting shows that eventually all the Eu^{2+} will be oxided to Eu^{3+} which is in agreement with our expectations.

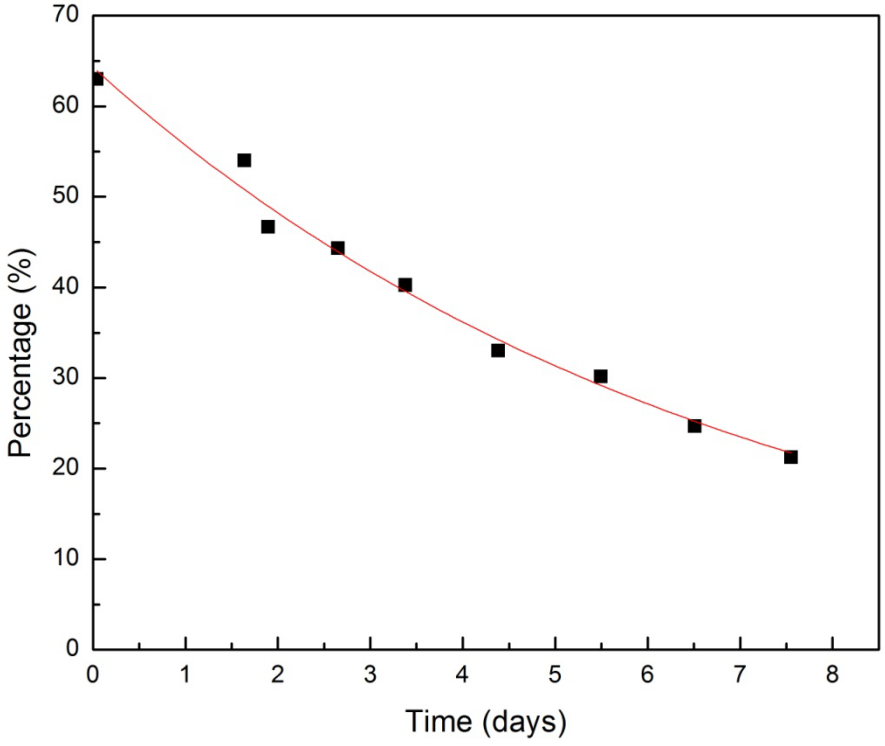

Figure 45 Percentage of Eu^{2+} in heated $EuCl_3$ over time. The data was fitted by $y = 64.3 \exp\left(-\frac{t}{6.9}\right)$ with t is the number of days.

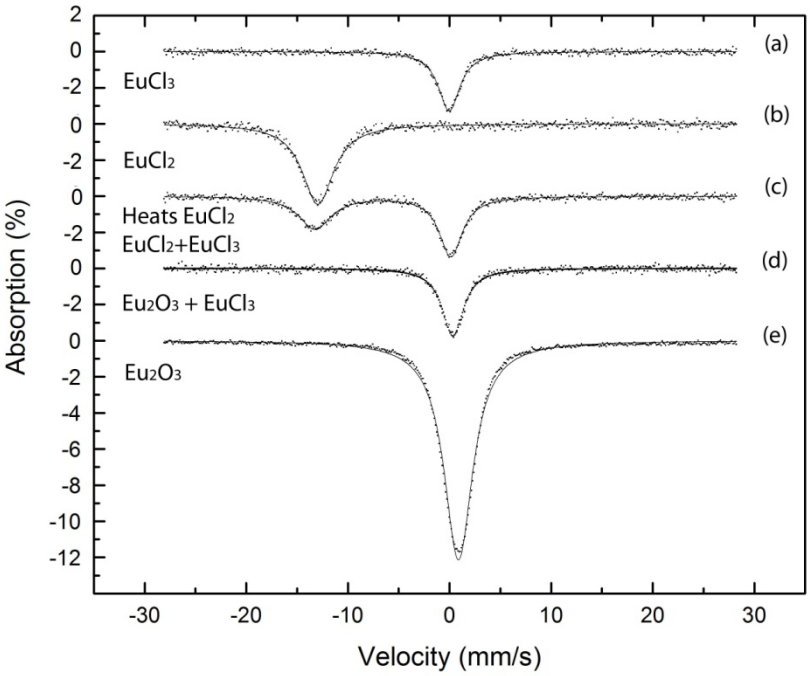

Figure 46 Mössbauer spectra of (a) pure $EuCl_3$, (b) pure $EuCl_2$, (c) $EuCl_2$ after heating contains $EuCl_2$+$EuCl_3$, (d) Heated $EuCl_2$ after30 days contains a mixture of Eu_2O_3+$EuCl_3$, and (e) pure Eu_2O_3

The initial pure $EuCl_3$ is shown in Figure 46a and has a chemical shift 0 mm/s, the initial pure $EuCl_2$ is shown in Figure 46b and has a chemical shift of 1 mm/s, in agreement with to reference [27]. Figure 46c shows the mixture of Eu^{2+} and Eu^{3+} after heated $EuCl_3$. Figure 46d shows the oxidation of $EuCl_2$ to a mixture of $EuCl_3$ and Eu_2O_3. $EuCl_2$ is in the unstable state and has the tendency to oxidize to Eu^{3+}. Eu^{2+} oxidizes to Eu^{3+} when it comes into contact with the oxygen and moisture from the atmosphere and becomes Eu_2O_3. The chemical shift of Eu_2O_3 is known to be around +1 mm/s. The chemical shift of $EuCl_3$ is known to be around 0 mm/s [27]. In Figure 46d, the chemical shift of the peak is around 0.8 mm/s. It is consistent with our hypothesis that the peak was made up of $EuCl_3$ with a chemical shift of 0 mm/s and Eu_2O_3 with a chemical shift of 1 mm/s.

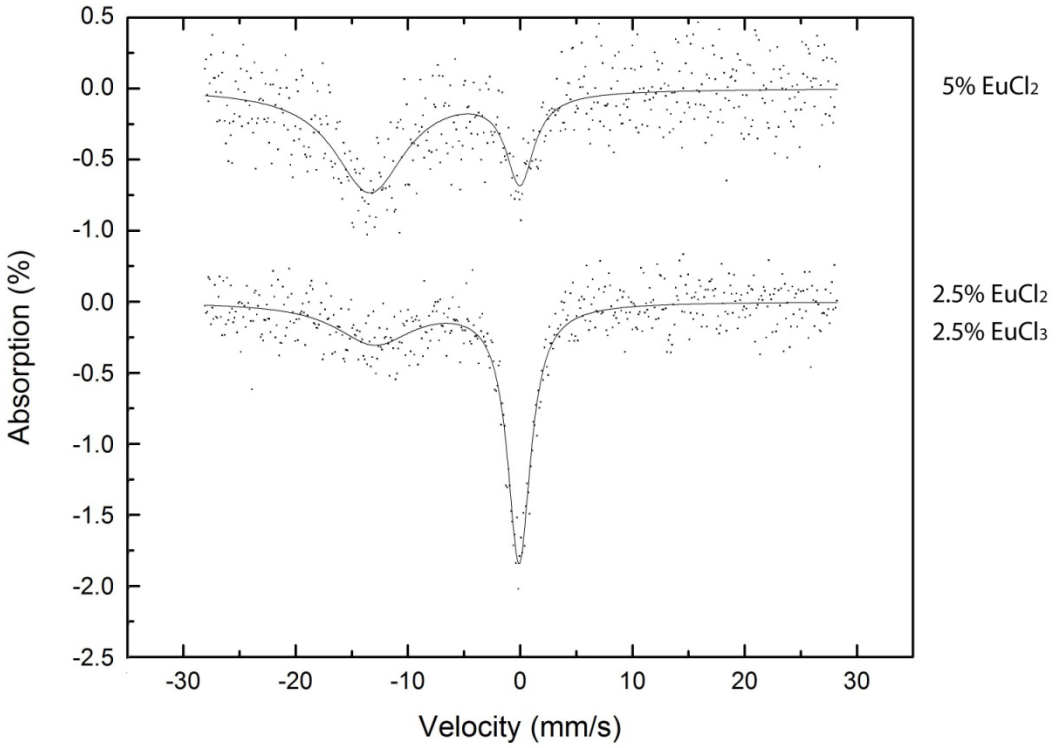

Figure 47 Mössbauer spectra of ZBLAN glass with 5 mole % Eu-doping. The sample of the top spectrum was doped with 5 mole % $EuCl_2$. The sample of the bottom spectrum was doped with 2.5 mole % $EuCl_2$ and 2.5 mole % $EuCl_3$

The more europium doping in the ZBLAN glass samples, the easier it is to observe the Mössbauer effect. However it is also more difficult to form a glass and excess europium reduces the quality of the glass samples. The less europium doping in ZBLAN glass samples, the harder it is to observe Mössbauer effect, as heavy Zirconium in the glass sample blocks most of the gamma rays. The 5 mole % doped of Eu sample was synthesized in order to study the ratio of Eu^{2+}/Eu^{3+} in the glass samples.

Figure 47 shows Mössbauer spectra of ZBLAN glass plates with 5 mole % Eu-doping. The ZBLAN glass samples were cut into plates of 10 mm × 10 mm × 1.6 mm (thickness). The plates were mechanically polished to a thickness of ~ 150 μm. Thin glass

plates were inserted in polythene bags and mounted on the sample holder in the Mössbauer instrument.

The top spectrum shows a sample that was doped with 5 mole % $EuCl_2$. The ratio of the areas under the peaks for Eu^{2+} and Eu^{3+} is 78:22. This indicates that 22% of Eu^{2+} was oxidized to Eu^{3+}. The bottom spectrum shows a sample that was doped with 2.5 mole % $EuCl_2$ and 2.5 mole % $EuCl_3$. The ratio of the areas under the peaks for Eu^{2+} and Eu^{3+} is 37:63, indicating 13% of the Eu^{2+} was oxidized to Eu^{3+}. The study shows that Eu^{2+} can exchange electrons with other elements to be oxidized to Eu^{3+} even during the careful sample preparation procedure.

CHAPTER IV
CONCLUSIONS AND RECOMMENDATIONS

Europium-doped ZBLAN glasses were studied to optimize the performance as an image plate for medical application. For this study, the Europium-doping level, the annealing time and temperature were varied. $BaCl_2$ nanoparticles were formed upon annealing. The annealing temperature was determined based on DSC measurements. XRD measurements show the formation of hexagonal $BaCl_2$ nanoparticles within the glass matrix of all samples at low annealing temperature and for short annealing time. The hexagonal $BaCl_2$ nanoparticles convert into orthorhombic $BaCl_2$ nanoparticles at higher temperature and longer annealing time.

Photoluminescence confirms the transformation from hexagonal phase $BaCl_2$ nanoparticles to the orthorhombic phase. As a result, the peak around ~ 410 nm shifts to ~ 400 nm and the peak around ~ 480 nm moves to lower energies. The study of secondary ion mass spectroscopy showed that the samples made at UTSI contained low amounts of oxygen. Oxygen which was found on the surface of those samples was attributed to contact with the brass mold obtained from the atmosphere outside the glove box. The study of ion chromatography and inductively coupled plasma showed that the loss of fluoride, chloride and other cations does not impair the plate performance.

Transmission electron microscopy was used to observe the growth of $BaCl_2$ nanoparticles. The size of $BaCl_2$ nanoparticles is bigger at longer annealing time. $BaCl_2$ nanoparticles were formed uniformly across the samples.

The Mössbauer spectroscopy study confirmed that part of the Eu^{2+} doping in ZBLAN glass was oxidized to Eu^{3+}, which reduces the luminescence of the image plate. $EuCl_3$ (99.99% purity) was heated to convert Eu^{3+} into Eu^{2+}. After one hour heating

$EuCl_3$ at 700°C, around 60% of Eu^{2+} and 40% of Eu^{3+} were observed. Eu^{2+} can be produced from Eu^{3+} in the laboratory environment to reduce the cost.

Future studies should include in situ x-ray diffraction should be considered to study the phase transformation of $BaCl_2$ nanoparticles. In situ XRD would help to determine the best annealing time and temperature. An “In situ” Mössbauer study would help to determine the ratio of Eu^{2+}/ Eu^{3+} as a function heating temperature. Low temperature Mössbauer spectroscopy would help to determine the ratio of Eu^{2+}/ Eu^{3+} under very low oxidation conditions.

LIST OF REFERENCES

1. Schweizer, S. and J.A. Johnson, *Fluorozirconate-based glass ceramic X-ray detectors for digital radiography*. Radiation Measurements, 2007. **42**(4-5): p. 632-637.
2. Chen, G., et al., *Insights into phase formation in fluorochlorozirconate glass-ceramic storage phosphors.* Applied Physics Letters, 2006. **88**(19).
3. Schweizer, S., et al., *New developments in X-ray storage phosphors.* Radiation Measurements, 2004. **38**(4-6): p. 633-638.
4. Schweizer, S. 2006 [cited 2011 Jan-20]; Available from: http://fb6www.uni-paderborn.de/ag/ag-schweizer/research/x-ray_storage_phosphors.html.
5. Schweizer, S. 2011; Available from: http://fb6www.uni-paderborn.de/ag/ag-schweizer/research.html.
6. Schweizer, S., et al., *Multi-functionality of fluorescent nanocrystals in glass ceramics.* Radiation Measurements, 2010. **45**(3-6): p. 485-489.
7. J.A. Johnson, M.V., J.K.R. Weber, *Unpulished work*, 2011.
8. Group, N. *The cost-effective starter instrument for quality assurance*. [cited 2011 Jan-21]; Available from: http://www.netzsch-thermal-analysis.com/en/products/detail/pid,1.html.
9. Twisp. *SIMS instrument scheme*. 2006 [cited 2011 Jan-21]; Available from: http://en.wikipedia.org/wiki/File:SIMS_instrument_scheme_600x600.png.
10. Johnson, J.A., et al., *Eu-activated fluorochlorozirconate glass-ceramic scintillators.* Journal of Applied Physics, 2006. **100**(3).
11. Abollino, O., et al., *Determination of zirconium, barium, lanthanum, aluminium, sodium, hafnium and fluorine in fluorozirconate glasses - Development of different dissolution procedures and analytical techniques.* Fresenius Journal of Analytical Chemistry, 1992. **343**(6): p. 482-487.
12. Harrington, J.A. *Infrared Fiber Optics*. [cited 2011 Mar 8]; Available from: http://irfibers.rutgers.edu/pdf_files/ir_fiber_review.pdf.

13. SPI. [cited 2011 Jan 24]; Available from: http://www.2spi.com/catalog/instruments/dimpler.shtml.
14. *Mossbauer spectroscopy*, ed. D.P.E. Dickson and F.J. Berry1986, Cambridge ; New York: Cambridge ; New York : Cambridge University Press.
15. Kauzmann, W., *THE NATURE OF THE GLASSY STATE AND THE BEHAVIOR OF LIQUIDS AT LOW TEMPERATURES.* Chemical Reviews, 1948. **43**(2): p. 219-256.
16. Schweizer, S., et al., *Photostimulated luminescence from fluorochlorozirconate glass ceramics and the effect of crystallite size.* Journal of Applied Physics, 2005. **97**(8).
17. Paßlick, C., et al., *Crystallization behavior of rare-earth doped fluorochlorozirconate glasses.* Journal of Non-Crystalline Solids. **In Press, Corrected Proof**.
18. Paßlick, C., et al., *Differential scanning calorimetry investigations on Eu-doped fluorozirconate-based glass ceramics.* Journal of Non-Crystalline Solids, 2010. **356**(52-54): p. 3085-3089.
19. Ji, L., et al., *Combined electron and focused ion beam system for improvement of secondary ion yield in secondary ion mass spectrometry instrument.* Applied Physics Letters, 2006. **89**(16).
20. Ji, Q., et al., *Combined electron- and ion-beam imprinter and its applications.* Applied Physics Letters, 2004. **85**(20): p. 4618-4620.
21. Kobayasi, T., et al., *FLUORESCENCE LIFETIME AND QUANTUM EFFICIENCY FOR 5D- 4F TRANSITIONS IN EU2+ DOPED CHLORIDE AND FLUORIDE-CRYSTALS.* Journal of Luminescence, 1980. **21**(3): p. 247-257.
22. Edgar, A., et al., *Structural phase changes in barium bromide nano-crystals in a fluorobromozirconate glass-ceramic x-ray storage phosphor.* Journal of Physics-Condensed Matter, 2001. **13**(28): p. 6259-6269.
23. Secu, M., et al., *Photostimulated luminescence from a fluorobromozirconate glass-ceramic and the effect of crystallite size and phase.* Journal of Physics-Condensed Matter, 2003. **15**(7): p. 1097-1108.

24. Ball, J., et al., *A MOSSBAUER-SPECTROSCOPY STUDY OF AN ANHYDROUS NON-STOICHIOMETRIC EUROPIUM(III) CHLORIDE PHASE.* Journal of the Less-Common Metals, 1983. **95**(1): p. 161-170.
25. MacFarlane, D.R., et al., *In situ generation of Eu2+ in glass-forming melts.* Journal of Non-Crystalline Solids, 1999. **257**: p. 53-58.
26. Coey, J.M.D., A. McEvoy, and M.W. Shafer, *MOSSBAUER STUDY OF EUROPIUM IN FLUOROZIRCONATE GLASS.* Journal of Non-Crystalline Solids, 1981. **43**(3): p. 387-392.
27. Grandjean, G.J.L.a.F., *Mossbauer spectroscopy applied to inorganic chemistry*, in *Modern Inorganic chemistry*. p. 513-590.

APPENDIX

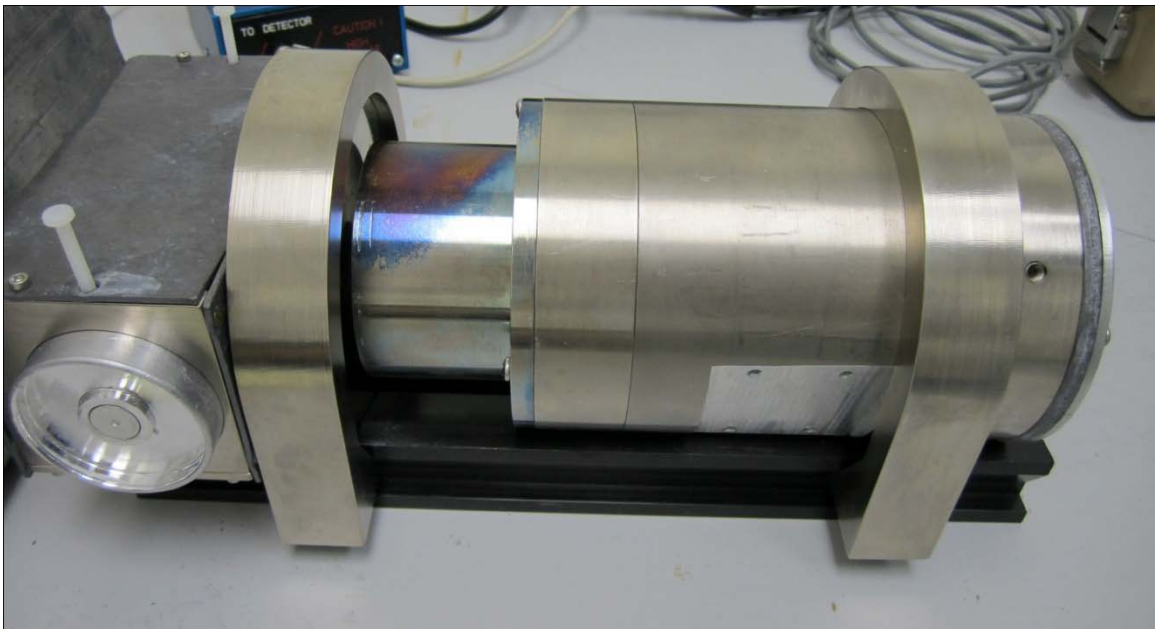

Figure 48 Mössbauer Apparatus

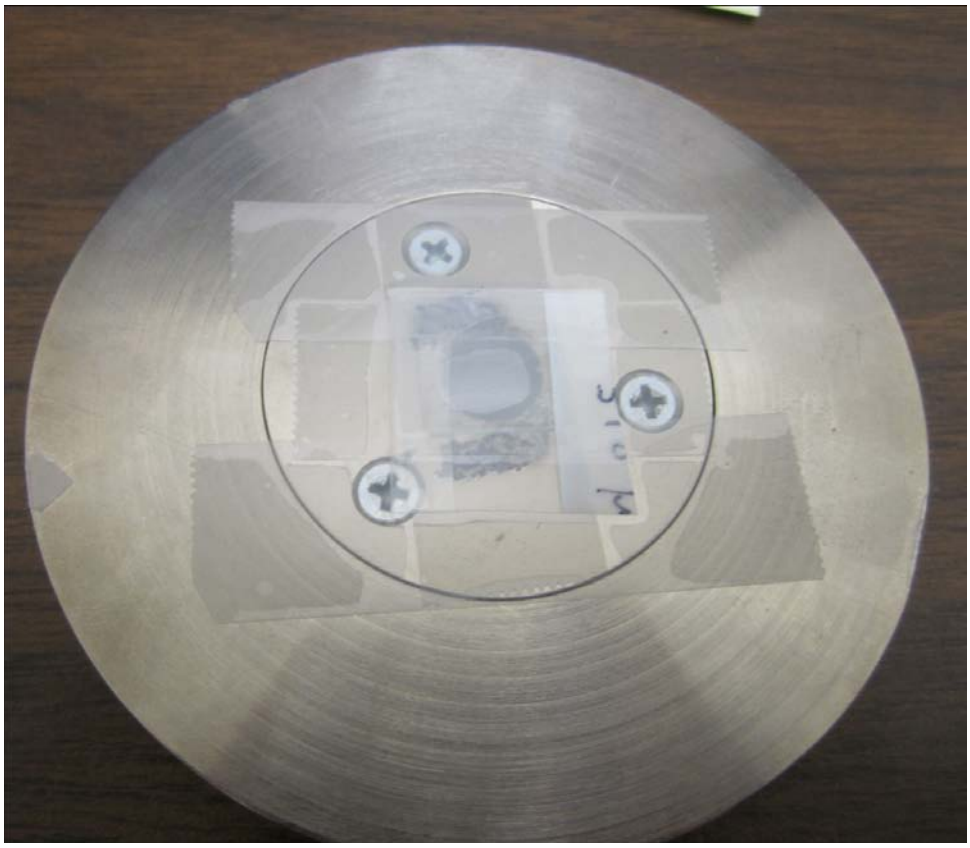

Figure 49 Mössbauer sample holder

VITA

Manh Vu was born in Hanoi, Vietnam on April 24, 1985. He graduated from Hanoi-Amsterdam High School, one of the most prestigious schools in the nation, specializing in Physics. He then continued his study in United States and received his Bachelor of Science Degree in Physics and Mathematics from Coe College in 2009. In fall 2009, he joined the University of Tennessee at Space Institute to pursue his Master of Science Degree in Materials Science. He worked closely as a graduate assistant of Doctor Jacqueline Anne Johnson.